



OPEN ACCESS

EDITED BY

Alcides Nobrega Sial,
Federal University of Pernambuco,
Brazil

REVIEWED BY

Martin J. Streck,
Portland State University, United States
Magdalena Matusiak-Malek,
University of Wroctaw, Poland

*CORRESPONDENCE

Shehata Ali,
shehata.ali@mu.edu.eg

SPECIALTY SECTION

This article was submitted to
Geochemistry,
a section of the journal
Frontiers in Earth Science

RECEIVED 17 April 2022

ACCEPTED 05 August 2022

PUBLISHED 07 September 2022

CITATION

Ali S, Abdallah SE, Abu Anbar MM,
Azzaz SA and Alrashidi KN (2022),
Petrology of continental, OIB-like,
basaltic volcanism in Saudi Arabia:
Constraints on Cenozoic anorogenic
mafic magmatism in the Arabian Shield.
Front. Earth Sci. 10:921994.
doi: 10.3389/feart.2022.921994

COPYRIGHT

© 2022 Ali, Abdallah, Abu Anbar, Azzaz
and Alrashidi. This is an open-access
article distributed under the terms of the
[Creative Commons Attribution License
\(CC BY\)](https://creativecommons.org/licenses/by/4.0/). The use, distribution or
reproduction in other forums is
permitted, provided the original
author(s) and the copyright owner(s) are
credited and that the original
publication in this journal is cited, in
accordance with accepted academic
practice. No use, distribution or
reproduction is permitted which does
not comply with these terms.

Petrology of continental, OIB-like, basaltic volcanism in Saudi Arabia: Constraints on Cenozoic anorogenic mafic magmatism in the Arabian Shield

Shehata Ali^{1*}, Shehta E. Abdallah², Mohamed M. Abu Anbar³,
Sayed A. Azzaz² and Khuloud N. Alrashidi⁴

¹Geology Department, Faculty of Science, Minia University, Minya, Egypt, ²Geology Department, Faculty of Science, Zagazig University, Zagazig, Egypt, ³Geology Department, Faculty of Science, Tanta University, Tanta, Egypt, ⁴Ministry of Education—State of Kuwait, Kuwait, Egypt

Continental basaltic volcanism in the Arabian Shield of Saudi Arabia has distinctive mineralogical and geochemical features important for understanding the composition of its mantle source and melting conditions. The studied Cenozoic basaltic rocks (19.3–15 Ma) occur at Jabal Al Gharib and Jabal Al Ghuraybayn areas within the Al Qasr quadrangle and southwest of Hail City in Saudi Arabia. They show similar chondrite-normalized REE patterns, suggesting that they were derived from a common mantle source. Their OIB-like features, silica undersaturated nature, and incompatible trace element ratios all reveal an asthenospheric mantle source and argue against crustal contamination process, subduction contribution, and interaction with a lithospheric mantle. Moreover, the elevated compatible trace element concentrations of Ni, Cr, and Co and the low and relatively narrow range of $\text{FeO}^{\text{total}}/\text{MgO}$ ratios argue for their nearly primitive nature and indicate that the role of crystal fractionation processes was minor during the evolution of the studied rocks. The estimated temperatures indicate that the sequence of crystallization likely began with olivine at 1,378–1,475°C, then clinopyroxene at 1,137–1,214°C, and soon after followed by plagioclase at 1,096–1,108°C. Plagioclase geo-hygrometers reveal 0.63–1.41 wt% water contents, suggesting crystallization under hydrous conditions. The basalts have geochemical features such as high $(\text{K}_2\text{O} + \text{Na}_2\text{O})/\text{TiO}_2$, Zr/Hf, and Nb/Ta ratios and negative K anomalies which suggest a carbonated peridotite mantle source. Their bulk-rock compositions are consistent with <5% CO_2 in their peridotite melts. Highly incompatible elemental ratios supported by REE modeling indicate that they were generated by low degrees (4–10%) of partial melting of a garnet-bearing lherzolite mantle source. The garnet signature in the source region suggests a deeper origin exceeding ~85 km. The basanite compositions fall within the range of alkaline OIB and intracontinental basalts formed in the rifted region. Moreover, they show geochemical characteristics typical of Cenozoic rift-related Oman basanites and other Arabian intraplate volcanic rocks. The basaltic volcanism in Saudi Arabia seems to be the result of melting asthenospheric mantle source in response to the lithospheric extension that is

spatially and temporally linked to Red Sea rifting and triggered anorogenic mafic magmatism due to passive mantle upwelling beneath the Arabian Shield.

KEYWORDS

basanite, asthenospheric mantle, Tertiary, anorogenic, mafic magmatism, Arabian Shield

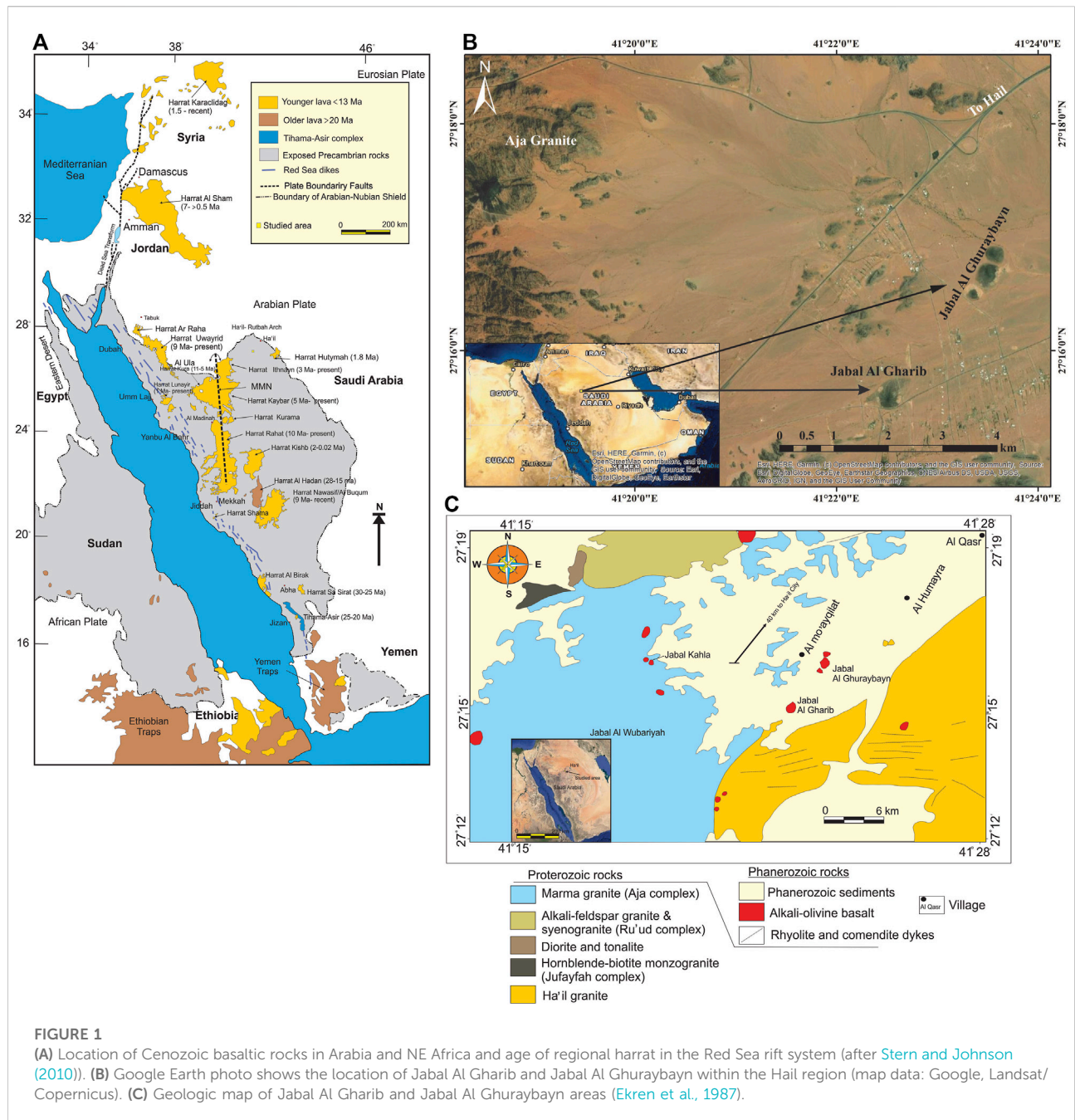
Introduction

Continental intraplate basaltic volcanism shows distinctive mineralogical and geochemical features important for understanding the subcontinental lithospheric mantle and the underlying asthenosphere. These features provide valuable information on the composition of their mantle source and melting conditions. Generally, the genesis of this intraplate alkaline mafic magmatism has been attributed to lithospheric extension and/or plume activity (Baker et al., 1996; Hofmann et al., 1997; Courtillot et al., 1999; Pik et al., 1999; Endress 2010; Ali and Ntafos 2011; Ali et al., 2013; Shallaly et al., 2013; Bosworth et al., 2015; Farahat et al., 2017). The Red Sea is one of the youngest continental intraplate magmatic regions (Figure 1A) trending NNW-SSE. It is a good example for understanding extensional tectonics in continental regions. The extension in the Red Sea region commenced ~30 Ma ago, separating African and Arabian continental plates and creating a new ocean basin (McKenzie et al., 1970; Girdler and Styles, 1974). This rift system represents an active zone of deformation that existed between the African and Arabian plates. In addition to active rift-related topographic features generated in the Red Sea region, its development involved abundant intrusion of dikes and sills, as well as extrusion of lava flows (Bosworth and Stockli, 2016) (Figure 1A). Pre-rift mafic lavas that erupted in Ethiopia, Eritrea, and southern Yemen at 31 Ma represent the earliest Red Sea region magmatism that was linked to the Afar plume (Stern and Johnson, 2019). The earliest rift-related magmatism included syn-rift mafic tholeiitic dike swarms, gabbros, and volcanic rocks formed between 24 and 20 Ma and extended over 3,000 km from northern Afar to northern Egypt (Bosworth and Stockli, 2016) and northern Jordan to southern Syria (Harrat Ash Shaam) (Ilani et al., 2001).

Middle Miocene magmatism continued after a 7–9 Ma quiescence in the Red Sea basin and formed new basaltic lavas at Harrat Ash Shaam (<13 Ma) as well as the younger harrats of Saudi Arabia (Nawasif/Al Buqum, Kishb, Rahat, Khaybar and Ithnayn, and Uwayrid) (Stern and Johnson, 2019). This resumed volcanism was attributed to sinistral movement along the Dead Sea transform fault and possibly reveals the emergence of upper mantle upwelling below the western Arabian Plate (Ilani et al., 2001). The recent volcanic and dike activity occurred at harrats Rahat and Lunayyir in the past 800 years and continued until the present (Pallister et al., 2010) in NW Saudi Arabia and E Jizan coastal plain. The Red Sea magmatism was sporadic and revealed low volume than other rifted margins (Bosworth and Stockli, 2016).

Oligocene flood basalt volcanism on the Afro-Arabian triple junction (i.e., Yemen, Ethiopia, Eritrea, and Djibouti) was linked to continental extension and perhaps the activity of mantle plume (Denielet et al., 1994; Chazot and Bertrand, 1995; Baker et al., 1996; Stewart and Rogers, 1996; Pik et al., 1999). Nevertheless, the geodynamic context and magma origin of much of the intraplate volcanism on the Arabian plate are unclear (Camp and Roobol, 1992). In the last 15 Ma, extensive intraplate lavas erupted along the western Arabian Peninsula (e.g., Jordan, Syria, Israel, Yemen, and Saudi Arabia), post-dating Africa and Arabia break-up, the Red Sea opening, and Oligocene flood basalt volcanism in Yemen and Ethiopia (Albarede, 1992; Baker et al., 1997). Late Cenozoic intraplate volcanism, although in fact extensive, is less voluminous than Oligocene flood basalt volcanism in Yemen and Ethiopia (12,000 km³ against 350,000 km³), revealing possibly lower mantle temperature or/and less lithospheric extension than the setting responsible for the voluminous flood volcanic province (White and McKenzie, 1989).

The Afar mantle plume was related to Oligocene flood basalt volcanism in Yemen and Ethiopia and influenced Pliocene to recent intraplate volcanism in Yemen (Baker et al., 1996; 1997; Pik et al., 1999). The Yemen late-stage intraplate volcanism was formed by small amounts of lithospheric extension resulting in the melting of shallow mantle formerly metasomatized by the Afar plume (Baker et al., 1997, 1998). However, the genesis of the magma and geodynamic context of northwestern Arabia volcanism far away from the Afar plume influence are not so clear. McKenzie and Bickle (1988) suggested that a normal mantle potential temperature of 1,280°C needs a stretching factor (initial/final lithosphere thickness) of 2–5 to initiate partial melting of the dry mantle. Camp and Roobol (1992) suggested that taking into consideration the small stretching factor, an anomalous hot mantle is necessary to produce alkaline volcanism in Saudi Arabia. They assumed that a part of the hot asthenosphere, thought to have initiated in the Afar region, may have been channeled NW through pre-existing lithospheric flexures (e.g., Ebinger and Sleep (1998)) or that a separate mantle plume occurred under Saudi Arabia. Conversely, Altherr et al. (1990) and Stein and Hofmann (1992) suggested that older shallow mantle sources formed alkaline basalts in Saudi Arabia and Israel. Stein and Hofmann (1992) hypothesized that an old “fossilized” plume head (4.2 Ga) was stored in the subcontinental lithosphere and that volcanic activity was periodically triggered by lithosphere thinning or rifting.



The Al Qasr quadrangle represents the northeastern part of the Arabian Shield and is situated southwest of Hail City in Saudi Arabia. The Cenozoic basaltic rocks formed within the Al Qasr quadrangle between 19.3 and 15 Ma and occur mostly in a long N 30° E trend (Stoeser and Elliott, 1985). The studied basaltic rocks are located in the Jabal Al Gharib and Jabal Al Ghuraybayn areas (Figures 1B, C), which belong to the Al Qasr quadrangle of Saudi Arabia. The present study introduces for the first time new geologic, petrographic, mineralogical, and geochemical data from these basaltic rocks located in both areas for a better understanding of

the nature of their asthenospheric mantle source and to provide insights into their tectonic settings and melting conditions.

Geological background

Regional geology

The Arabian–Nubian Shield (Figure 1A), one of the largest tracts of juvenile crust on the Earth, was produced by the

accretion of arcs that occurred between East and West Gondwana major fragments during the Neoproterozoic time (Stern, 2002; Johnson and Woldehaimanot, 2003; Meert, 2003; Stoesser and Frost, 2006; Abu-Alam et al., 2013; Ali and Alshammari, 2021). The Arabian Shield of Saudi Arabia represents a segment of the Arabian–Nubian Shield outcropping as a predominant juvenile Neoproterozoic crust on the eastern side of the Red Sea rift (Figure 1A) and is covered in the east by Phanerozoic sedimentary rocks (Nasir and Stern, 2012; Ali and Alshammari, 2021). It has been relatively stable since the late Neoproterozoic time, and it was rejuvenated during several tectonic phases between the late Precambrian and Tertiary (Nasir and Stern, 2012; Witte et al., 2017). The last time of rejuvenation was during the Red Sea opening in the last 30 Ma (Farahat et al., 2017; Witte et al., 2017; Farahat and Ali, 2019).

The Al Qasr quadrangle covers a region of about 2,750 km² in the northeastern part of the Arabian Shield. It is situated between latitudes 27°00' N and 27°30' N and longitudes 41°00' E and 41°30' E in the southwest of Hail City. The studied Jabal Al Gharib and Jabal Al Ghuraybayn areas are located about 40 km southwest of Hail City (Figures 1B, C) within the Al Qasr quadrangle.

All rock units in the quadrangle, except Cenozoic olivine basaltic rocks, belong to the late Proterozoic to early Cambrian Arabian Shield (Stoesser and Elliott, 1985). The Cenozoic rocks occur as a field of basaltic plugs and necks striking north. The Precambrian units comprise volcanic and plutonic rocks. The mafic volcanic rocks (metabasalts) were documented in Banana unit (<735 Ma), whereas the felsic ones (rhyolitic volcanics) were observed in Hadn unit (613 Ma). The plutonic rocks (735–570 Ma) prevail in the quadrangle and comprise four major groups (Stoesser and Elliott, 1985). The oldest group consists mainly of diorite, quartz-diorite, tonalite, and granodiorite and is probably related to the banana unit. The second group consists of foliated monzogranites and syenogranites, formed during an episode of regional deformation in the Hail region. The third one represents the most extensive group of intrusive rocks which form small to major batholiths of weakly deformed to undeformed biotite ± hornblende granites and granodiorites in the northeastern part of the Arabian Shield. The Hadn volcanic rocks are the extrusive equivalent of these rocks. The last group comprises widespread alkali feldspar, alkali granites, and alkali rhyolite dikes which occur in the northeastern part of the Arabian Shield.

The dioritic to tonalitic rocks are interpreted to be related to an island-arc stage. The foliated granitic rocks are probably related to a major episode of continental collision in the Arabian Shield (Stoesser and Elliott, 1985). Voluminous intraplate granites were formed after the initial collision. The alkali granitic rocks were emplaced, after the culmination of the intraplate plutonism, during regional extension related to the Najd Fault system in the Hail region.

The Cenozoic basaltic rocks occur as a field of volcanic pipes and necks and comprise twenty-seven mapped intrusions within

the Al Qasr quadrangle (Stoesser and Elliott, 1985). The majority occur along a broad N 30° E axis from the southwest to the north corners of the quadrangle. Their sizes range from a few tens of meters to 0.9 km in diameter. Lherzolite xenoliths, up to a few centimeters in diameter, were recorded in one of these plugs. Basaltic rocks gave an age range of 19.3–15 Ma based on the whole rock K/Ar age dating (Stoesser and Elliott, 1985). These dates likely indicate one or more episodes of Miocene volcanic activity in the Hail region along the axis of the Hail arch (Greenwood, 1974); the products of the volcanic activity were mostly removed by erosion.

Local geology

Both the Jabal Al Gharib and Jabal Al Ghuraybayn areas (Figure 1B) show nearly similar field geological characteristics (Figure 2). The areas comprise basaltic and granitoid rocks surrounded by Phanerozoic sediments (Figure 1C). Cenozoic basaltic rocks at Jabal Al Gharib occur as a single isolated conical-shaped hill (Figure 2A), whereas those at Jabal Al Ghuraybayn are represented by three conical-shaped hills (Figure 2F) with nearly moderate relief. These basalts follow a common NE trend (Figures 1B, C) typical of most Cenozoic basaltic rocks in the Al Qasr quadrangle. They erupted within the exposed Precambrian rocks in the Arabian Shield of Hail region (Figures 1, 2BH). A rhyolitic dyke (Figure 2C) intruded by basaltic rocks is observed at Jabal Al Gharib. Basaltic rocks show polygonal columnar joints (Figure 2D), which are common at Jabal Al Gharib. The rocks of both areas are characterized by spheroidal weathering (Figures 2E, I), forming spheroidal basaltic boulders at the top of the flows. This type of weathering results from expansion during chemical weathering of systematically jointed, massive rocks and is associated with onion-skin peeling (Figures 2E, I). Some vesicular basaltic rocks are observed in the upper parts of the flows. The vesicles are sometimes filled with secondary minerals (zeolites, calcite, quartz, or chalcedony), forming an amygdaloidal structure. Mantle xenoliths are not found in both areas. The surrounding granitoid rocks comprise the Marma granite (Aja complex), alkali-feldspar granite, syenogranite (Ru'ud complex), diorite and tonalite, hornblende-biotite monzogranite (Jufayfah complex), and Hail granites (Figure 1C). Rhyolite and comendite dykes cut across Hail granites (Figure 1C). The Phanerozoic sediments are Quaternary surficial deposits represented by eolian sand dunes and alluvial deposits.

Analytical methods

Major element compositions of minerals (Supplementary Tables S1–S4) were determined using an electron microprobe (JXA-8230) at the State Key Laboratory of Continental

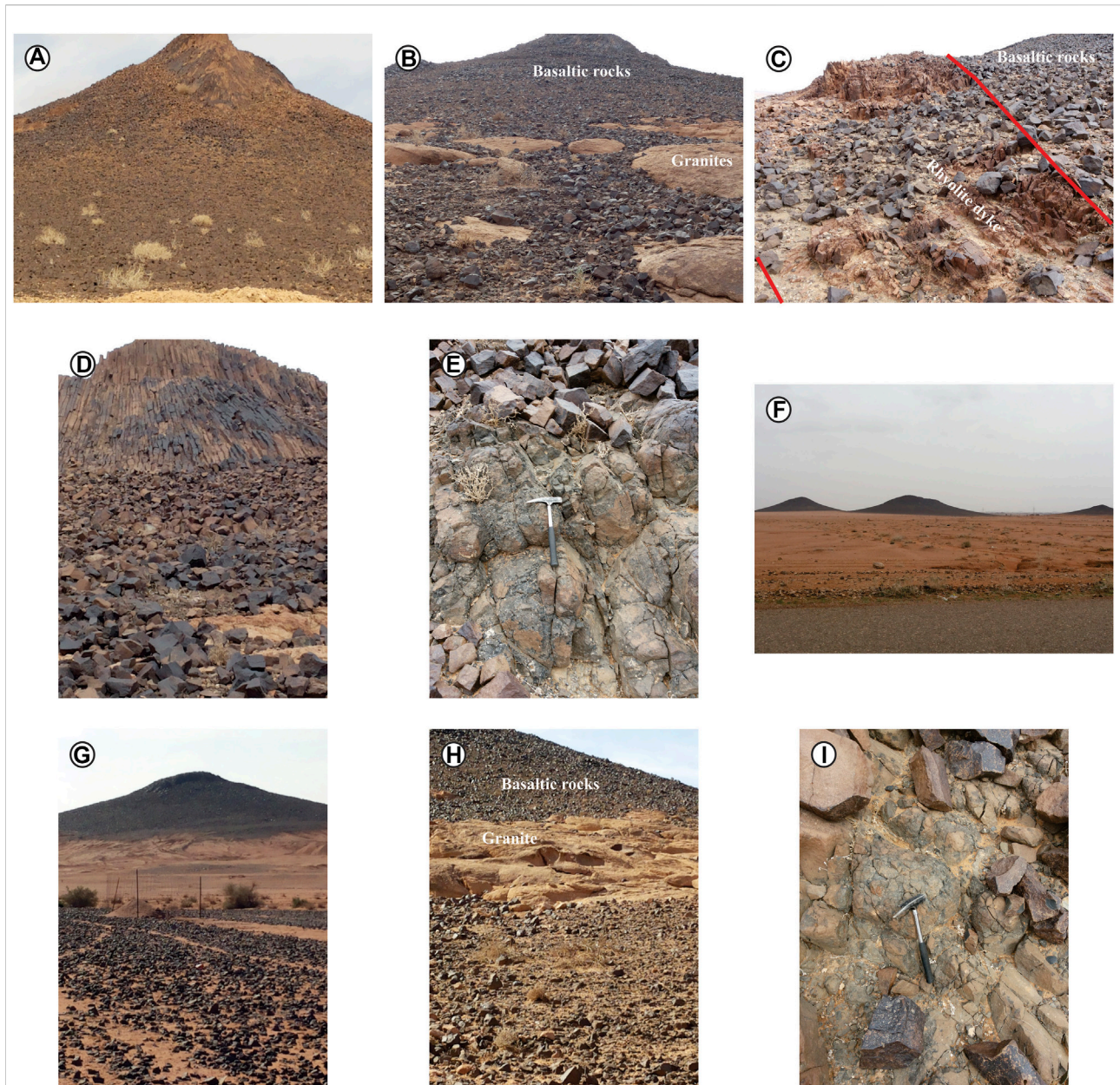


FIGURE 2

Field photographs show (A) general view of Jabal Al Gharib, (B) basaltic rocks erupted on granitic rocks at Jabal Al Gharib, (C) rhyolitic dyke cut through basaltic rocks of Jabal Al Gharib, (D) columnar basaltic rocks in Jabal Al Gharib, (E) spheroidal weathering on basaltic rocks of Jabal Al Gharib, (F) general view of Jabal Al Ghuraybayn, (G) close view of Jabal Al Ghuraybayn, (H) basaltic rocks erupted on granitic rocks at Jabal Al Ghuraybayn, and (I) onion-like peeling in basalt boulders of Jabal Al Ghuraybayn.

Dynamics, Northwest University, Xian, China. The instrument was operated at an acceleration voltage of 15 kV, a beam current of 10 nA, and a beam diameter of 2 μm . The total electron microprobe error is 1%–2% for major elements. All analyses were carried out against standards of natural and synthetic phases, and standard correction procedures were applied.

Twenty-two representative fresh rock samples were analyzed for major and trace elements (Table 1). The analyses were carried

out at the State Key Laboratory of Continental Dynamics, Northwest University, Xian, China. The analytical procedures for the major elements were as follows: 0.7 g sample powders were mixed with 3.6 g $\text{Li}_2\text{B}_4\text{O}_7$, 0.3 g LiF, 0.4 g NH_4NO_3 , and 2–3 drops of 1.5% (w/w) LiBr solution. The mixture was put into a platinum (Pt 95% + Au 5%) crucible and melted in a high-frequency melting instrument into a glass disk before analysis. Then, the glass beads were analyzed by XRF (Rigku RIX2100).

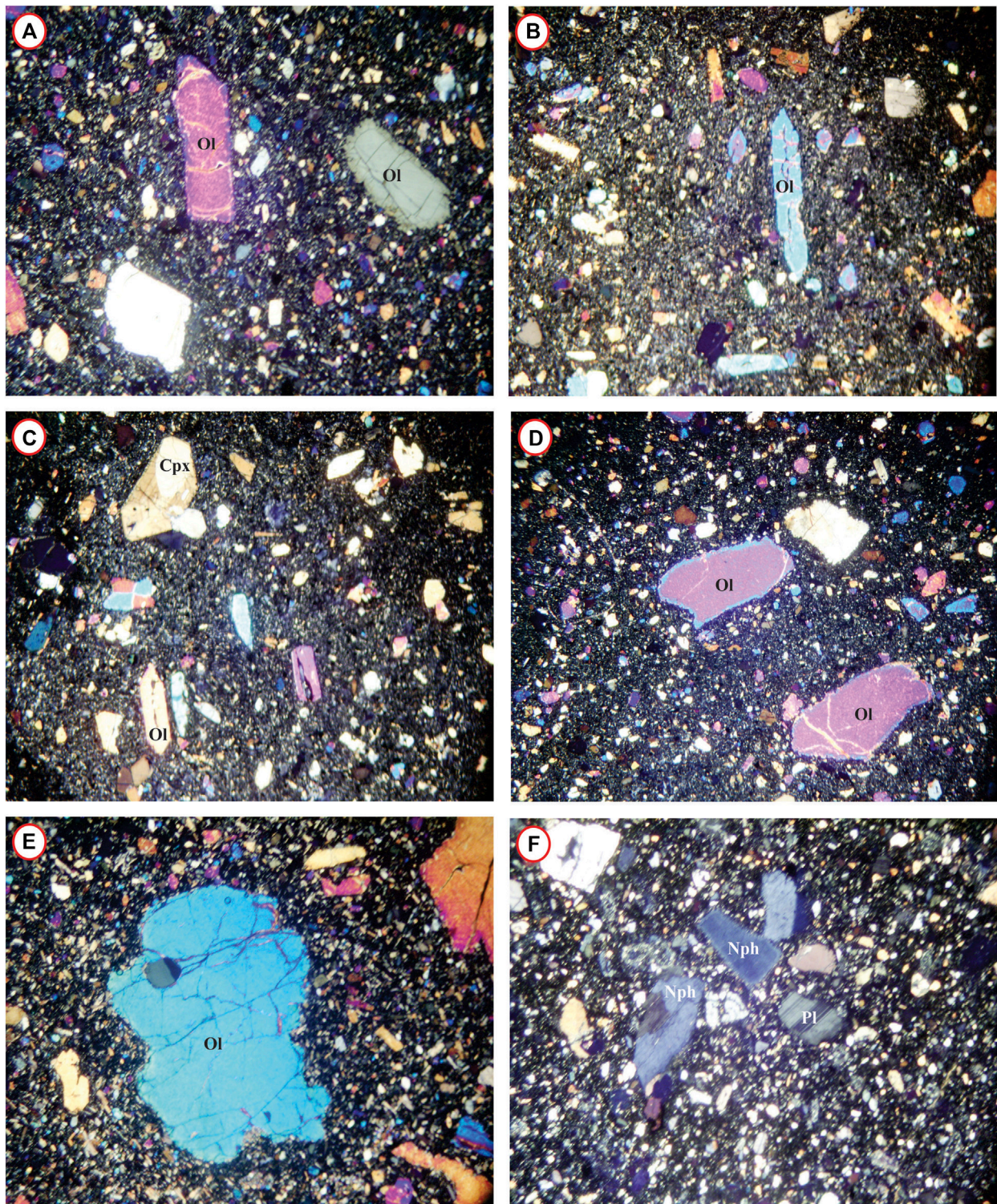


FIGURE 3

Photomicrographs of basanites showing the main petrographic features. (A) Prismatic euhedral olivine phenocryst with characteristic porphyritic texture; (B) seriate texture showing a range of crystal sizes. Note the elongated skeletal olivine in the center, and (C) sector zoning in clinopyroxene. Note the six-sided euhedral olivine phenocryst with prism and dome faces on the left side; (D) sub-rounded olivine xenocrysts. Few rounded olivine microphenocrysts are also present on the top. Note the compositional zoning in xenocrysts with sawtooth edges; (E) anhedra olivine xenocryst; (F) plagioclase microphenocryst with characteristic polysynthetic twinning surrounded by nepheline microphenocrysts. Abbreviations: Ol, olivine; Pl, plagioclase; Cpx, clinopyroxene; Nph, nepheline. Magnification x50, XPL.

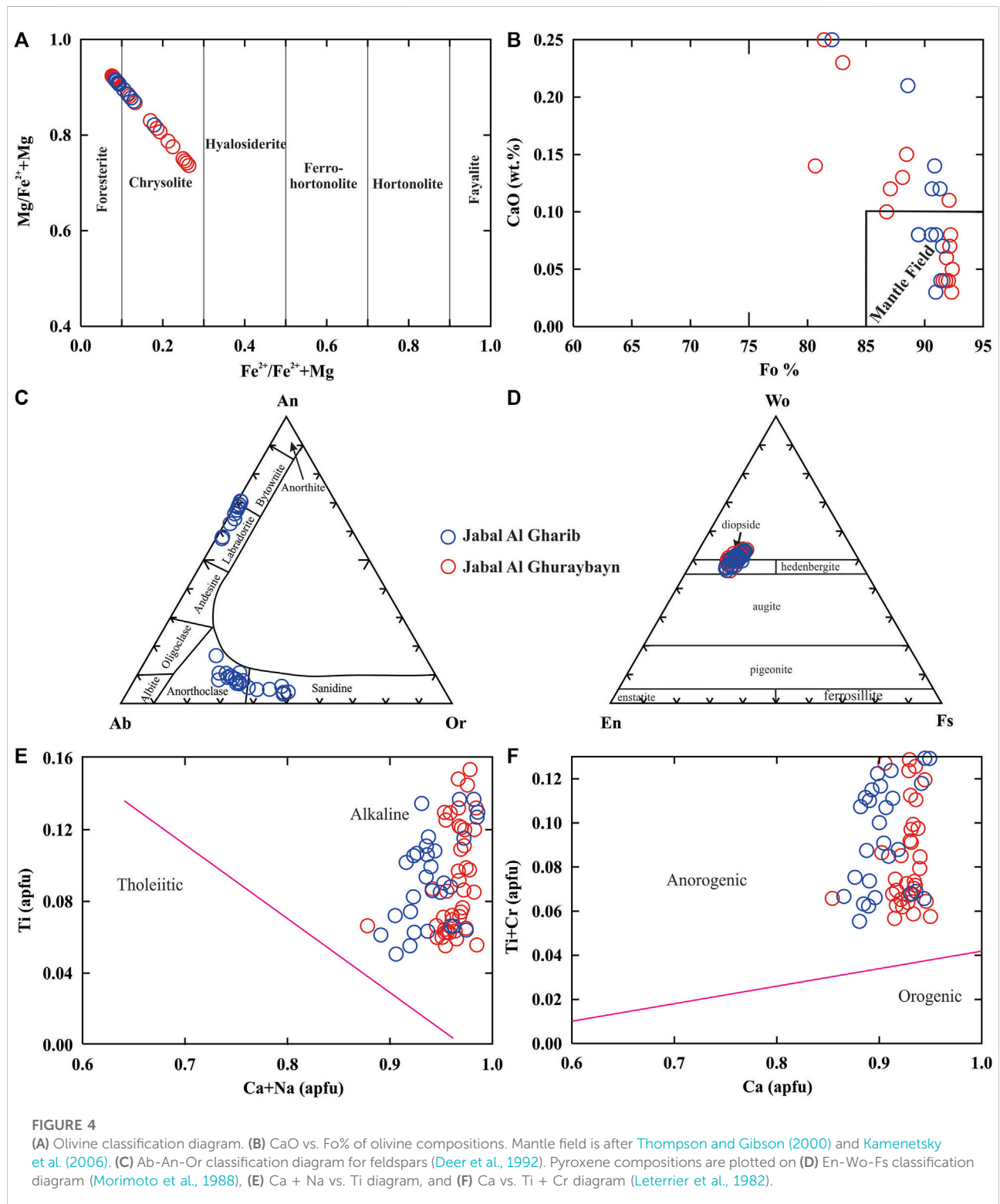
TABLE 1 Bulk-rock geochemical analyses.

Area	Jabal Al Gharib											Jabal Al Ghuraybayn											
	Sample No.	G1	G2	G3	G4	G6	G7	G8	G10	G11	G13	G13R	Gh3	Gh4	Gh5	Gh6	Gh7	Gh7R	Gh14	Gh15	Gh19	Gh20	Gh23
Major oxides (wt.%)																							
SiO ₂	41.58	41.69	41.47	42.05	42.02	42.63	42.12	42.94	42.86	42.44	42.63	42.05	43.32	41.84	42.09	43.42	43.41	44.42	42.05	42.08	41.90	44.17	
TiO ₂	2.52	2.59	2.54	2.45	2.41	2.42	2.38	2.51	2.53	2.52	2.52	2.91	2.40	2.83	2.90	2.92	2.92	2.23	2.59	2.56	2.61	2.36	
Al ₂ O ₃	13.31	12.17	13.27	12.60	12.11	12.60	12.36	13.49	13.41	12.82	12.86	14.76	12.70	14.45	14.85	13.96	13.45	12.76	12.56	12.70	12.43	12.95	
Fe ₂ O ₃ ^{total}	14.09	13.35	14.11	13.14	12.97	13.12	12.91	12.64	12.67	12.91	12.90	13.24	12.71	13.15	13.51	13.65	13.62	12.17	13.26	13.17	13.29	12.46	
MnO	0.19	0.18	0.19	0.19	0.19	0.19	0.19	0.19	0.19	0.18	0.18	0.19	0.19	0.19	0.20	0.20	0.20	0.18	0.18	0.19	0.19	0.18	
MgO	9.92	13.14	9.82	12.48	13.71	12.33	13.41	10.61	10.86	11.81	11.84	10.44	13.07	11.18	10.18	10.33	10.98	11.60	11.96	11.67	12.31	11.34	
CaO	9.76	9.79	10.10	9.79	9.61	9.41	9.49	9.92	9.92	9.70	9.72	9.39	9.43	9.40	8.56	8.51	8.52	9.08	9.87	9.84	10.10	9.31	
Na ₂ O	4.80	3.79	4.42	3.99	3.90	4.12	3.90	3.99	4.04	3.94	3.91	3.96	3.30	3.70	4.26	4.34	4.36	3.81	3.79	4.24	3.76	4.03	
K ₂ O	1.28	1.29	1.13	1.30	1.34	1.32	1.22	1.53	1.49	1.45	1.45	1.53	1.15	1.46	1.49	1.51	1.51	1.45	1.58	1.45	1.36	1.34	
P ₂ O ₅	0.67	0.60	0.66	0.64	0.59	0.59	0.60	0.71	0.70	0.59	0.59	0.55	0.48	0.55	0.56	0.56	0.56	0.63	0.62	0.60	0.59	0.56	
LOI	1.54	1.16	1.86	0.96	0.87	0.80	1.20	1.28	1.17	1.17	1.17	0.68	1.09	0.96	1.03	0.33	0.32	1.65	1.20	1.10	1.12	1.18	
Total	99.66	99.75	99.57	99.59	99.72	99.53	99.78	99.81	99.84	99.53	99.77	99.70	99.84	99.71	99.63	99.73	99.85	99.98	99.66	99.60	99.66	99.88	
Trace elements (ppm)																							
Li	8.48	5.76	8.81	6.21	7.14	9.20	12.3	8.65	7.89	6.36	6.15	6.96	6.82	8.31	7.24	8.54	8.45	16.5	5.39	9.06	7.06	8.96	
Be	2.07	2.08	2.09	2.14	2.04	2.01	2.17	2.38	2.36	2.13	2.09	1.9	1.7	1.82	1.91	1.88	1.88	2.16	2.06	2.19	2.11	2.08	
Sc	18.4	20.2	19.0	20.4	21.2	21.1	20.7	23.7	24.1	20.4	20.2	19.5	25.1	19.4	20	20.1	20.3	18.8	21.0	20.6	21.1	20.0	
V	196	195	200	190	194	191	191	193	196	195	194	208	235	204	200	204	204	180	203	194	201	187	
Cr	187	380	186	364	478	378	447	331	340	339	331	269	604	346	199	202	207	338	335	308	345	334	
Co	68.9	69.7	68.9	73.8	79.1	74.3	77.4	67.1	65.0	73.8	73.6	65.1	75.1	59.4	57.4	56.7	57.3	62.3	73.1	72.2	78.0	67.4	
Ni	189	353	190	331	397	335	392	260	261	300	301	172	381	203	90.7	91.8	92.7	303	299	279	304	298	
Cu	61.7	59.9	68.6	65.2	64.8	62.2	63.0	64.8	65.3	64.2	63.3	46.1	71.5	48.6	53	54.8	55.1	56.9	62.4	66.5	63.9	60.5	
Zn	122	104	124	106	102	104	103	99.1	97.2	103	103	90.6	92.8	89.6	93.8	93.9	98.3	108	106	106	110	111	
Ga	22.2	21.3	22.6	21.5	20.8	21.0	21.0	21.1	21.2	21.7	21.6	19.6	18.8	19.1	20.1	20.2	20.2	21.4	21.7	21.8	21.7	21.1	
Ge	1.32	1.34	1.34	1.34	1.35	1.36	1.36	1.40	1.39	1.33	1.31	1.41	1.44	1.4	1.43	1.42	1.45	1.32	1.33	1.37	1.37	1.37	
Rb	12.2	22.1	12.9	22.5	24.2	16.7	22.6	23.9	24.3	25.4	25.4	24.4	19.6	25.8	20.6	21	20.8	18.1	23.9	21.6	21.8	11.8	
Sr	1076	850	1044	946	802	818	817	984	976	887	878	827	650	974	766	778	783	864	866	1035	952	801	
Y	21.2	21.5	21.8	23.0	22.3	22.7	22.7	27.9	27.6	22.2	22.3	24.4	21.9	24	24.8	24.7	25.1	23.1	22.7	23.4	23.3	22.8	
Zr	242	245	251	251	246	243	256	289	288	243	244	209	189	207	217	216	220	246	248	251	245	229	
Nb	83.0	92.5	84.5	95.2	89.3	87.5	94.8	129	128	91.7	91.4	93.2	80.8	91.4	92	90.2	90.1	85.3	90.7	94.5	89.1	84.1	
Cs	0.31	0.41	0.34	0.29	0.39	0.35	0.51	0.32	0.37	0.30	0.30	0.28	0.26	0.33	0.22	0.25	0.26	0.59	0.30	0.33	0.30	0.37	
Ba	436	477	423	468	415	442	461	461	442	436	433	333	311	330	337	340	341	481	503	480	467	516	
La	41.1	40.9	42.2	44.7	41.5	40.9	42.6	48.1	47.9	41.8	41.7	34.9	36.3	34.2	34	34	34.5	45.5	41.5	41.0	40.8	40.4	

(Continued on following page)

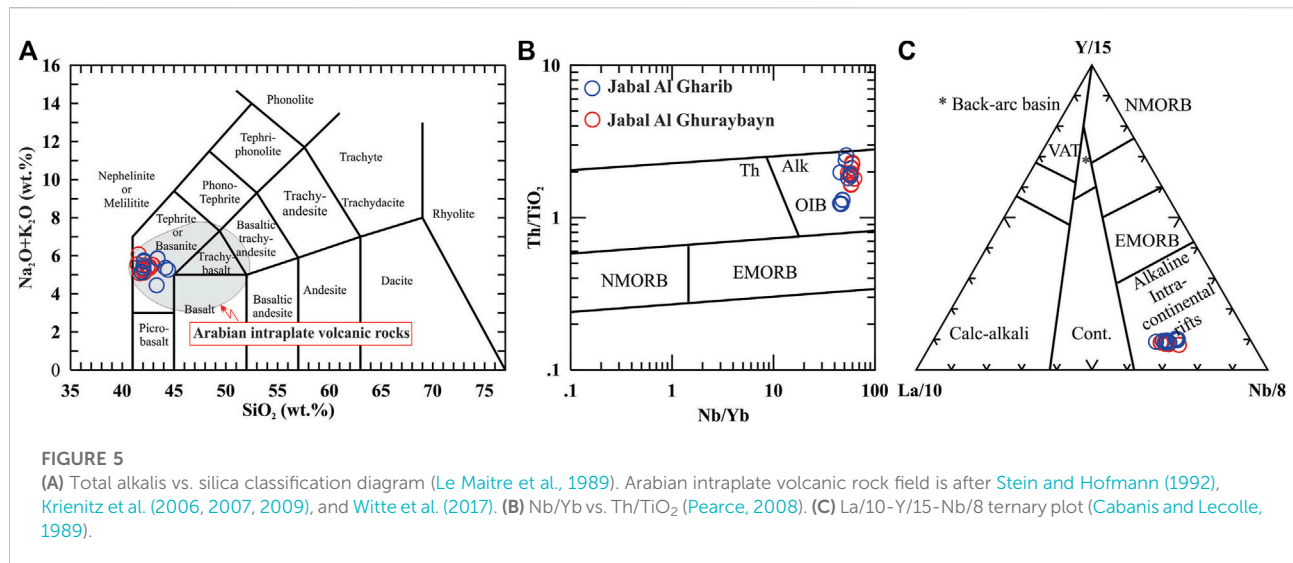
TABLE 1 (Continued) Bulk-rock geochemical analyses.

Area	Jabal Al Gharib										Jabal Al Ghuraybayn											
Ce	80.6	77.8	82.6	83.4	77.9	77.4	80.8	91.5	91.1	79.2	79.0	70.9	70.1	70.1	70.5	70.5	71.5	86.8	78.8	79.6	78.3	76.9
Pr	9.46	8.85	9.68	9.46	8.89	8.80	9.09	10.3	10.3	8.95	8.93	8.45	7.94	8.32	8.44	8.39	8.56	9.79	8.94	9.16	9.08	8.85
Nd	38.4	35.5	39.5	37.6	35.6	35.3	36.2	40.7	40.7	35.9	35.9	34.4	31.6	34	35.2	34.9	35.1	39.2	36.2	36.5	36.3	35.2
Sm	7.57	6.92	7.72	7.21	6.92	6.85	6.95	7.77	7.69	6.91	6.95	6.74	6.09	6.67	6.86	6.86	6.97	7.47	7.07	7.07	7.12	6.78
Eu	2.46	2.21	2.50	2.32	2.22	2.22	2.25	2.52	2.50	2.23	2.21	2.23	1.99	2.2	2.27	2.28	2.31	2.28	2.26	2.29	2.28	2.16
Gd	6.89	6.39	7.03	6.63	6.39	6.41	6.45	7.20	7.19	6.36	6.37	6.2	5.64	6.14	6.36	6.42	6.45	6.70	6.47	6.49	6.50	6.24
Tb	0.91	0.86	0.92	0.90	0.87	0.87	0.88	0.99	0.98	0.86	0.86	0.88	0.79	0.86	0.89	0.89	0.9	0.89	0.87	0.89	0.89	0.86
Dy	4.67	4.59	4.80	4.82	4.70	4.71	4.73	5.49	5.44	4.64	4.64	4.86	4.35	4.78	4.92	4.89	4.92	4.78	4.70	4.82	4.85	4.70
Ho	0.79	0.80	0.81	0.85	0.83	0.84	0.84	1.00	0.99	0.82	0.82	0.9	0.8	0.88	0.91	0.9	0.92	0.84	0.82	0.86	0.86	0.84
Er	1.95	2.01	1.98	2.14	2.10	2.13	2.14	2.63	2.61	2.07	2.06	2.33	2.13	2.31	2.4	2.38	2.4	2.12	2.08	2.17	2.17	2.14
Tm	0.25	0.26	0.26	0.28	0.27	0.28	0.28	0.35	0.35	0.27	0.27	0.33	0.29	0.32	0.33	0.33	0.33	0.27	0.27	0.29	0.29	0.28
Yb	1.43	1.48	1.45	1.61	1.58	1.62	1.63	2.16	2.14	1.59	1.57	1.94	1.77	1.91	1.96	1.96	1.99	1.63	1.57	1.66	1.64	1.63
Lu	0.20	0.21	0.20	0.23	0.22	0.23	0.23	0.31	0.31	0.22	0.22	0.28	0.26	0.28	0.29	0.28	0.29	0.23	0.22	0.23	0.23	0.23
Hf	5.38	5.69	5.50	5.68	5.71	5.57	5.79	6.03	5.98	5.62	5.65	4.84	4.41	4.74	4.92	4.92	5	5.61	5.78	5.94	5.95	5.40
Ta	5.08	5.81	5.16	5.97	5.76	5.49	6.03	7.07	6.98	5.79	5.73	5.7	4.92	5.47	5.44	5.37	5.41	5.10	5.67	5.98	5.82	5.21
Pb	1.98	2.71	2.14	3.14	2.64	3.39	3.04	3.94	3.44	3.20	3.12	2.35	2.73	2.21	2.83	2.57	2.54	4.06	3.69	3.49	3.31	3.89
Th	4.13	4.67	4.21	5.19	4.67	4.73	5.01	5.78	5.70	4.94	4.93	3.79	4.75	3.71	3.57	3.57	3.62	5.72	4.88	4.91	4.73	5.61
U	1.19	1.32	1.21	1.48	1.33	1.36	1.50	1.69	1.63	1.40	1.39	1.14	1.39	1.12	1.06	1.05	1.04	1.64	1.34	1.45	1.45	1.48



For trace element analyses, 50 mg sample powders were digested using HNO_3 , HF, and HClO_4 in polytetrafluoroethylene (PTFE) bombs with steel sleeves heated in an electronic oven at 190°C for 48 h. The final solutions, diluted to 80 g using 2% HNO_3 with an

internal standard (10 ng/g Rh in the solution), were analyzed using ICP-MS (Agilent 7500a). Analyses of USGS rock standards (BCR-2, BHVO-1, and AVG-1) indicate that the precision and accuracy are better than 5% for major elements and 10% for trace



elements. The detailed analytical procedures are found in the study by Liu et al. (2014).

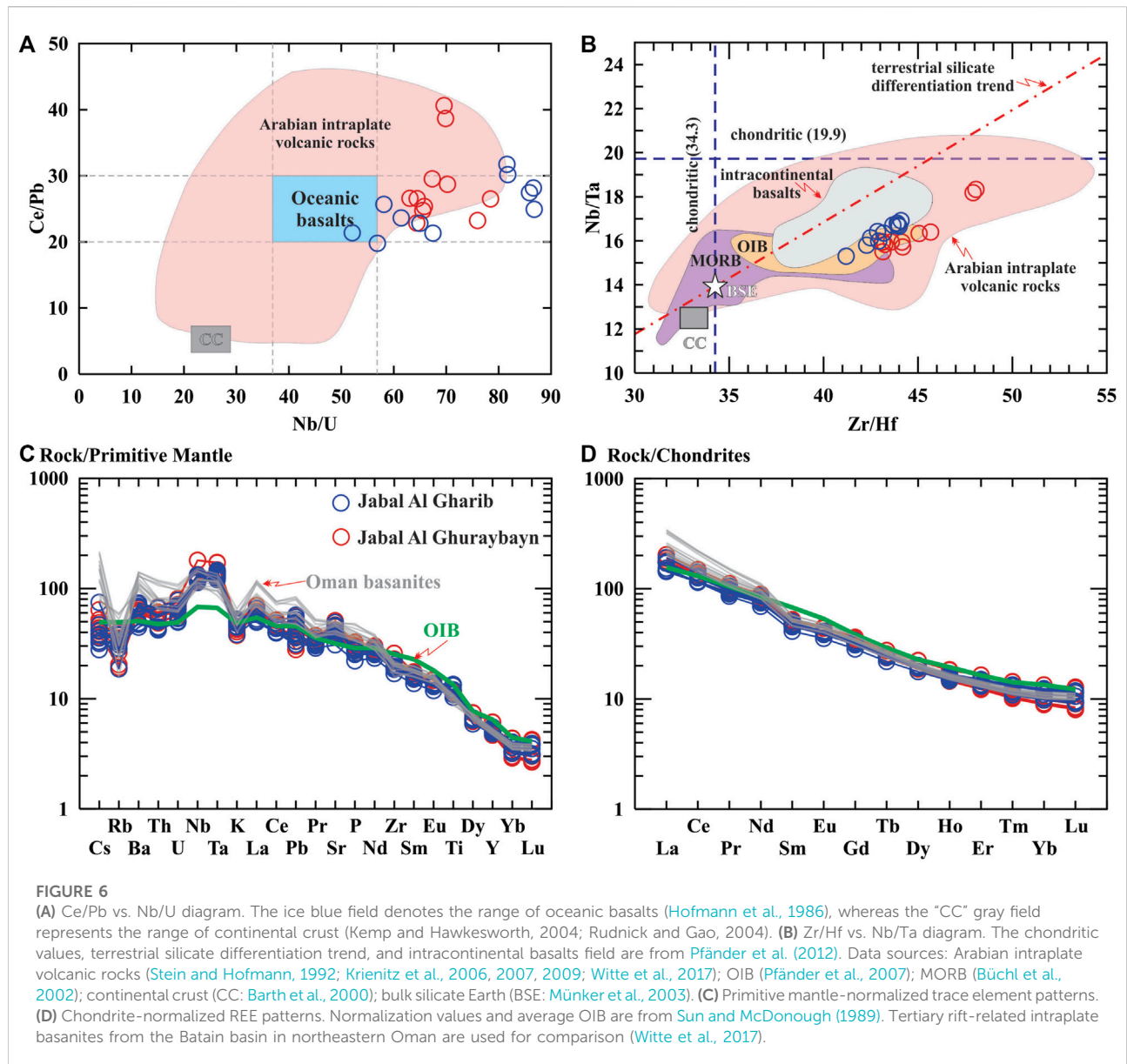
Petrography

Both the Al Gharib and Al Ghuraybayn basaltic rocks show identical petrographic characteristics (i.e., similar textural features and mineral assemblages). The rocks are fresh, mostly massive, dark-colored, and mainly olivine-phyric (Figures 3A–C). They exhibit mostly porphyritic and seriate textures (Figures 3A–C). The mineral assemblage comprises olivine, clinopyroxene, and plagioclase feldspar, together with a feldspathoid (Figure 3). The latter is more abundant than plagioclase feldspar and includes mainly nepheline with subordinate leucite. Lesser Fe-Ti oxides such as ilmenite and magnetite and minor alkali feldspars are also present. The suitable petrographic term for these rocks is basanite because the abundance of feldspathoids over plagioclase feldspars distinguishes them from olivine basalt and the presence of essential olivine distinguishes them from tephrite. Olivine is a fresh, colorless, euhedral to subhedral crystal with characteristic high relief. Olivine crystals are common as phenocrysts (–20–30 modal%) and in the groundmass (Figures 3A–C). The phenocrysts of olivine can be distinguished from mantle xenocrysts by morphologic and compositional (e.g., Fo and Ca; see mineral chemistry section) variations. Olivine phenocrysts occur as prismatic, rounded, and elongated skeletal crystals (Figures 3A–C). Sometimes, they show the characteristic six-sided euhedral shape in sections through the prism and dome faces (Figures 3B, C). Compositional zoning is usually observed in olivine crystals (Figures 3A, B). Minor olivine grains show angular to sub-rounded shapes and distinct zoning with sawtooth

edges (Figures 3D, E), suggesting that they represent mantle xenocrysts (e.g., Kamenetsky et al., 2006). Clinopyroxene crystals are euhedral to subhedral prismatic crystals that sometimes show sector zoning (Figure 3C). They are present as phenocrysts (–10–15 modal%) but are common in the groundmass. Plagioclase and alkali feldspars are present as minor phenocrysts (Figure 3F) but show lath-shaped crystals in the groundmass together with feldspathoid. Usually, plagioclase feldspars show characteristic polysynthetic twinning and are associated with feldspathoids (Figure 3F). The groundmass is composed of very fine-grained olivine, clinopyroxene, Fe-Ti oxides, interstitial plagioclase, nepheline, and glass.

Mineral chemistry

Mineral compositions of the analyzed minerals (olivine, clinopyroxene, plagioclase, alkali feldspar, and nepheline) are shown in Supplementary Tables S1–S4. Olivine compositions are classified as forsterite and chrysolite (Figure 4A). The phenocrysts of olivine are Mg-rich with a high Fo_{88.6–73.6} (Supplementary Table S1). Their high CaO contents (>0.1 wt%) suggest a magmatic origin (Figure 4B) (Thompson and Gibson, 2000). Vinet et al. (2015) showed that the most primitive olivines with forsterite contents up to Fo₉₀ and even the deformed ones are not from the mantle but have a magmatic origin. The most fayalitic olivine contains nearly similar contents of MnO and CaO (0.50 wt%) but is higher than the most forsteritic olivine (0.17 wt% and 0.21 wt%, respectively). On the other hand, olivine xenocrysts are present in some samples and show distinctive low CaO content (less than 0.1%) with compositions (Fo_{92.4–90.6}) characteristic of depleted mantle peridotites (Figure 4B) (Thompson and Gibson,

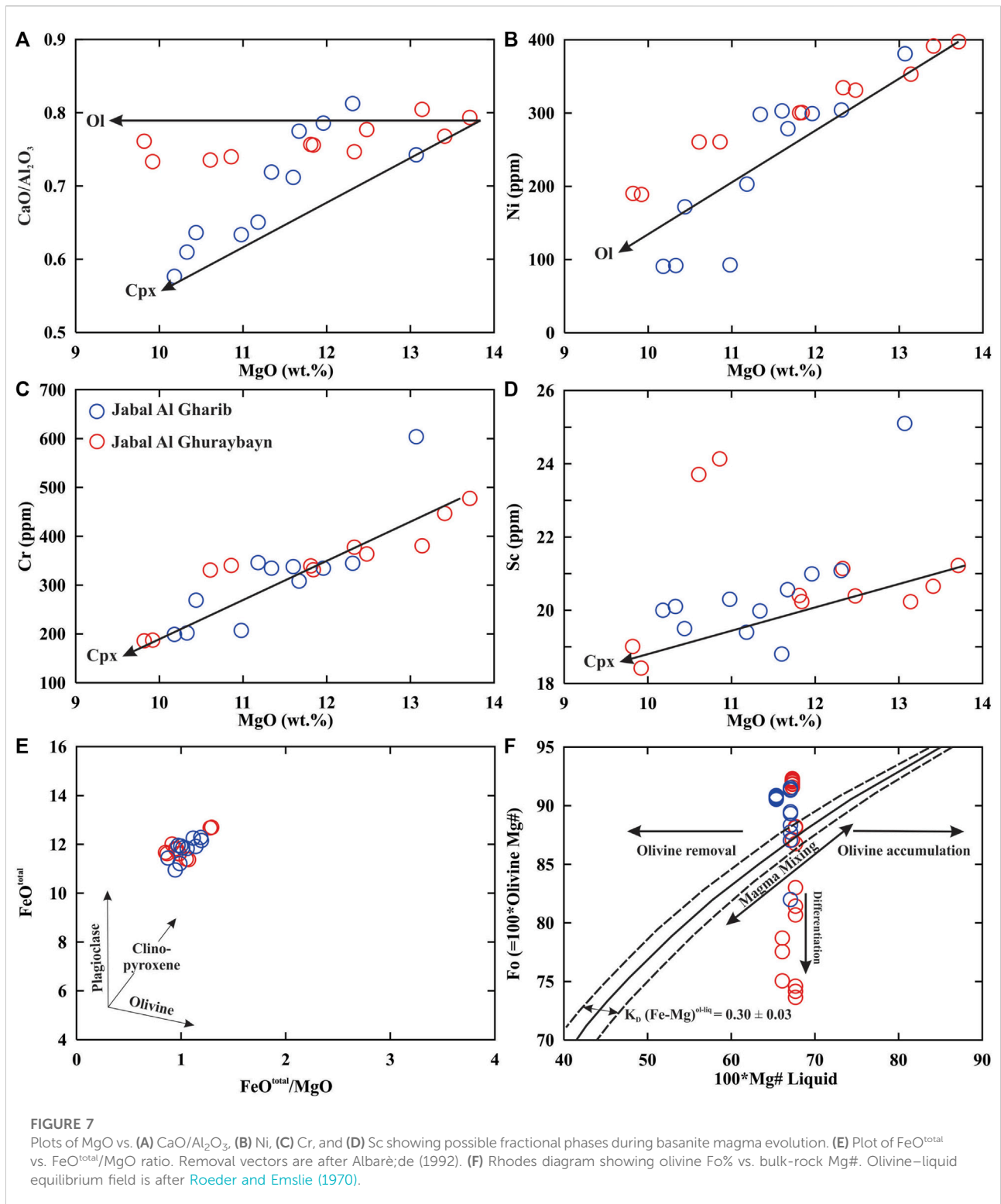


2000). The analyzed olivine xenocrysts are not further included in the discussion. Similar olivine xenocryst compositions were recorded in alkaline basalts from Burgenland, Austria (Ali and Ntafos, 2011).

Feldspars comprise both plagioclase feldspar and alkali feldspar (Supplementary Table S2) (Figure 4C). Plagioclase feldspar is more common than alkali feldspar in the studied basanites. It is represented by labradorite with An content ranging from An_{57.5–70.6}. Alkali feldspar consists of sanidine and anorthoclase with compositions ranging from Ab_{47.4}Or_{48.6}An_{4.0} to Ab_{66.3}Or_{25.4}An_{8.2}. It is plotted close to the Ab-Or joint and exhibits a systematic increase in Or contents with decreasing An contents (Figure 4C).

Pyroxene is represented by clinopyroxene (Supplementary Table S3) with Mg# (Mg number = Mg/Mg + Fe²⁺) varying between 0.76 and 0.89. It is diopside based on the Morimoto et al. (1988) classification (Figure 4D) and has compositions of Wo_{46.1–53.5}, En_{32.1–41.8}, and Fs_{10.4–14.9}. It shows a wide range of TiO₂ (1.8–5.38 wt%) and Al₂O₃ (4.86–11.84 wt%), which probably indicates different generations of clinopyroxenes. Its compositions are comparable to those present in alkaline anorogenic basaltic rocks (Figures 4E, F).

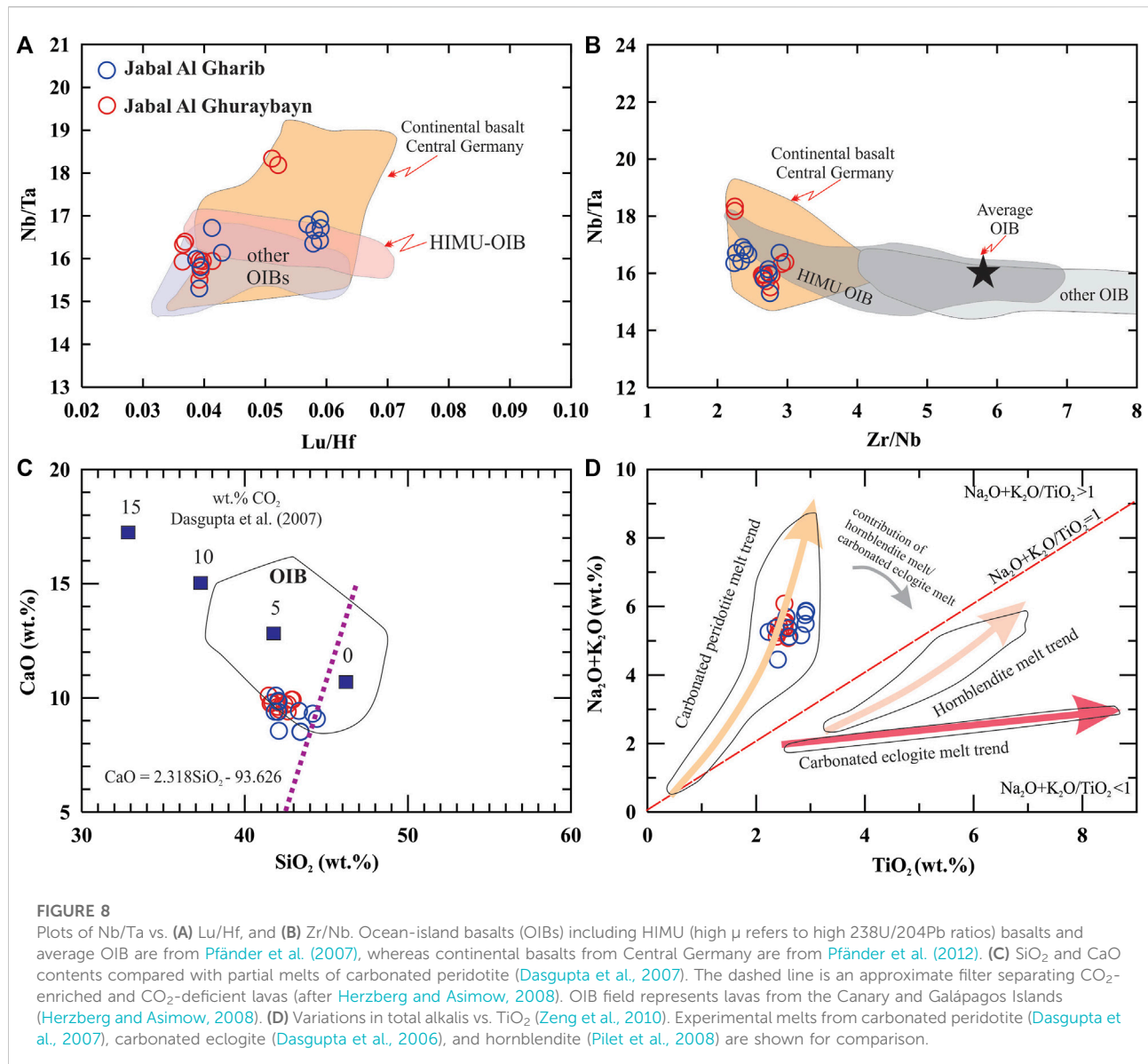
Feldspathoid in the studied basanites is represented by nepheline (Supplementary Table S4). It is composed mainly of Na₂O, 10.08–15.89 wt%; Al₂O₃, 32.19–35.00 wt%; and SiO₂, 43.42–48.52 with low K₂O, 3.09–4.25 wt% content.



Bulk-rock chemistry

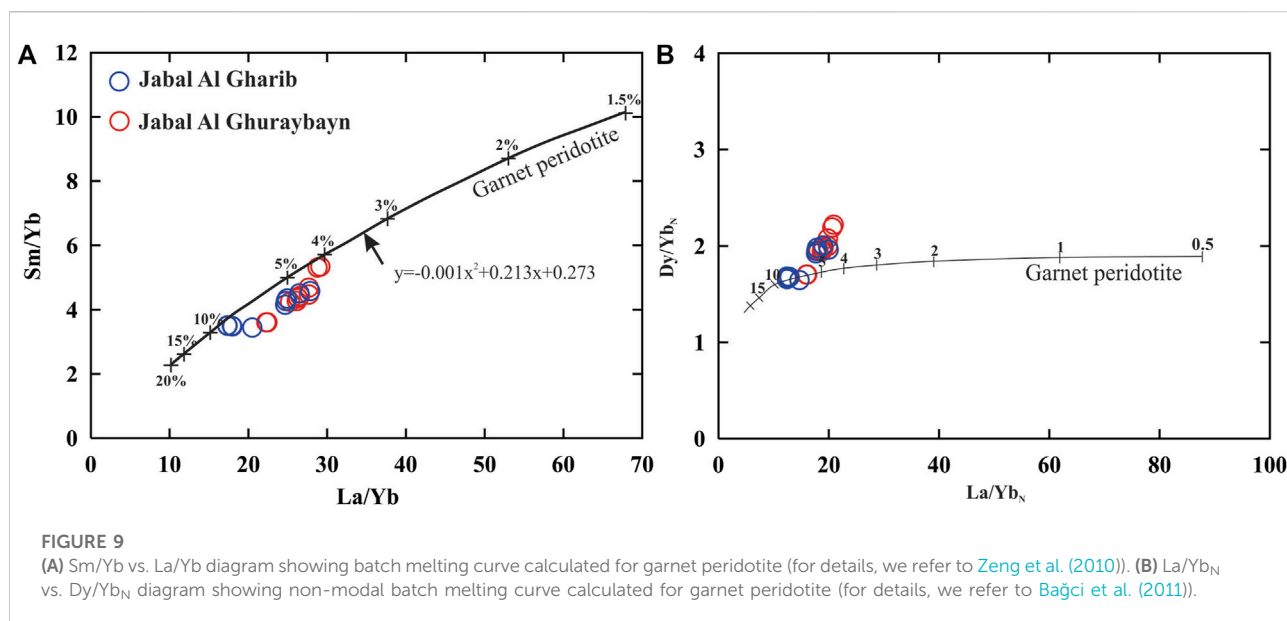
All rock samples show a homogeneous and limited range of compositions (Table 1). Their normative nepheline contents are

10.7–22.9 wt%, and those of olivine are 16.8–23.9 wt%. On the TAS diagram (Figure 5), their compositions fall into the tephrite-basanite field. The presence of olivine (normative >10 wt%) makes basanite a proper term. They have SiO₂ contents of



41.5–44.2 wt%, total alkalis between 4.5 and 6.1 wt%, MgO between 9.8 and 13.7 wt%, and TiO_2 between 2.2 and 2.9 wt%. The silica and alkali contents are comparable to those of other Arabian intraplate volcanic rocks (Figure 5A). They have compositional characteristics like alkaline OIB and intracontinental basalts (Figures 5B, C). Their Mg number values [$100 \text{ Mg}/(\text{Mg} + \text{Fe}^{2+})$] are high (58.0–67.7; mostly >60), and $\text{FeO}^{\text{total}}/\text{MgO}$ ratios are low (0.9–1.3). They are sodic, with $\text{Na}_2\text{O}/\text{K}_2\text{O}$ ratios >1 , typical for anorogenic mafic lavas (Lustrino and Wilson, 2007). These geochemical features overlap those from the circum-Mediterranean anorogenic Cenozoic primitive mafic rocks (Lustrino and Wilson, 2007). They have high but variable compatible trace element concentrations (ppm) of Ni (90.7–397.4), Cr (185.9–604), and

Co (56.7–79.1). These characteristic high MgO, Ni, and Cr contents in basanites are consistent with primitive mantle-derived melts; an inference supported by high Fo content in olivine ($\text{Fo}_{89.5-73.6}$) and Mg# (0.8–0.9) of clinopyroxene. The incompatible trace element ratios show relatively variable ranges (e.g., $\text{Ba}/\text{Nb} = 3.5-6.1$; $\text{La}/\text{Nb} = 0.4-0.5$; $\text{Ce}/\text{Pb} = 19.8-40.6$; $\text{Nb}/\text{U} = 52.1-86.8$; $\text{Zr}/\text{Nb} = 2.2-3.0$; $\text{Th}/\text{Ta} = 0.7-1.1$; $\text{Ta}/\text{Yb} = 2.7-3.9$). The Ce/Pb and Nb/U ratios are comparable to those in the Arabian intraplate volcanic rocks (Figure 6A). The Zr/Hf ratios (41.2–48.1) are higher than chondritic values ($\text{Zr}/\text{Hf} = 38$; Anders and Grevesse, 1989) but are within the range of continental and oceanic intraplate basaltic rocks (Figure 6B) (38–87; Dupuy et al., 1992). These rocks show Nb/Ta ratios (15.3–18.3) (Figure 6B)



below chondritic values (19.9 ± 0.6) but relatively higher than the ocean–island basalts (OIB: 15–16) (Pfänder et al., 2012). The Nb/Ta ratios are also higher than continental crust (CC: 12–13) and bulk silicate Earth (BSE: ~14) but like continental basalts (Figure 6B) (e.g., Central Germany: 15.0–19.1; Pfänder et al., 2012).

The primitive mantle-normalized trace element patterns (Figure 6C) are characterized by peaks at the HFSE (Nb–Ta) and negative K anomalies. They are variably enriched in LILE (Cs, Ba, and Sr) and commonly depleted in Rb. The rocks show patterns comparable to average OIB but with more enrichment in Nb and Ta. The Nb–Ta peak and K trough characterize anorogenic mafic rocks. The chondrite-normalized REE diagram (Figure 6D) shows an LREE-enriched pattern ($La/Yb_N = 12.4\text{--}20.9$) without Eu and Ce anomalies. Moreover, the REE patterns are identical to those of the average OIB. Generally, the trace element and REE patterns of both areas are similar (Figures 6C, D) and are identical to Cenozoic rift-related intraplate basanites from the Batain basin in northeastern Oman (Figures 6C, D) (Witte et al., 2017).

Discussion

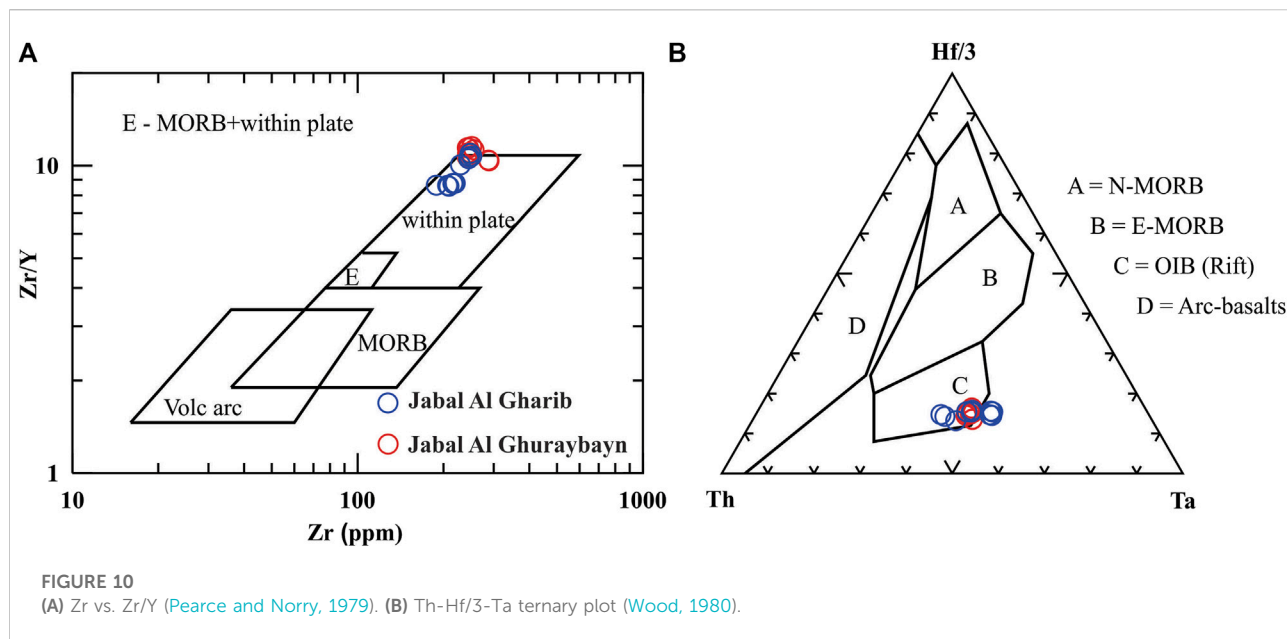
Post-magmatic alteration and contamination processes

The very low LOI contents (0.3–1.9 wt%) are consistent with the fresh nature of the rock samples and argue against post-magmatic alteration (Table 1). Additionally, the sub-chondritic Nb/Ta ratios (15.3–18.3; Figure 6B) and the absence of Ce anomalies in the chondrite-normalized REE patterns

(Figure 6D) support this inference (Polat and Hofmann, 2003). The Ba (311–516 ppm) and Sr (650–1,076 ppm) concentrations along with the Ce/Pb and Nb/U ratios (Figure 6A) are higher than in the continental crust, excluding contamination with crustal materials (Hofmann et al., 1986; Rudnick et al., 2003). Also, the low Th/Nb (0.17–0.20) and Rb/Nb (0.14–0.28) ratios are inconsistent with crustal contamination during the magma genesis of the studied rocks (Chazot and Bertrand, 1995; Taylor and Mclenman, 1995; Rudnick et al., 2003). The Nb/Ta ratios are higher than continental crust and BSE but comparable to the OIB-like basalts, supporting this implication (Figure 6B) (Pfänder et al., 2012). Moreover, the very low La/Nb ratios preclude significant contamination with continental crust materials or/and contribution from subduction components (Rudnick and Fountain, 1995; Condie, 1999). In conclusion, their OIB-like characteristics (e.g., Figure 6) and the undersaturated nature (nepheline normative with low silica contents) together with the incompatible trace element ratios argue against a role of crustal contamination process and/or interaction with lithospheric mantle (Smith et al., 1999; Zeng et al., 2010; Ali and Ntaflou, 2011; Ali et al., 2013). Therefore, the geochemical data of the studied rocks should reveal the nature of their mantle source.

Crystal fractionation processes and crystallization conditions

All the studied rock samples show high MgO contents (>9.5 wt%) and Mg# (mostly >60 and up to 68), suggesting a relatively primitive nature. Moreover, the high Fo contents of



olivine compositions indicate that they were crystallized from the relatively primitive mantle-derived melt. The range of Mg#, Cr, Co, and Ni contents (Table 1) likely indicates olivine and pyroxene fractionation. MgO content variation with CaO/Al₂O₃ ratios (Figure 7A) reveals fractionation of olivine and clinopyroxene. The decrease in Ni, Cr, and Sc with decreasing MgO supports this implication (Figures 7B–D). The absence of Eu anomalies in the REE patterns (Figure 6) argues against a role for plagioclase fractionation. Moreover, as pointed out by Albarède (1992), plagioclase post-melting fractionation is of restricted significance in OIB. The apparent liquid lines of descent based on Albarède (1992) removal vectors indicate the dominance of clinopyroxene over olivine fractionation (Figure 7E); however, in general, both clinopyroxene and olivine fractionation are minor. Since these lavas are silica undersaturated (nepheline normative with low silica <45 wt%) with high MgO contents, major crystal fractionation en route to the surface can be excluded. Moreover, the elevated compatible trace element concentrations of Ni, Cr, and Co and the low range of FeO^{total}/MgO ratios (Figure 7E) support this implication and indicate that the role of crystal fractionation processes was minor during the evolution of the studied rocks. This is consistent with the high Fo contents of olivine (Fo_{89.5–73.6}) and Mg# (0.76–0.89) of clinopyroxene.

The Rhodes diagram represents important tests of olivine–liquid equilibrium (Figure 7F). The olivine crystals and coexisting bulk-rock compositions are in equilibrium when the assumed olivine–liquid pair project along the solid line, within some determined error limit [K_D (Fe-Mg)^{ol-liq} = 0.30 ± 0.03]. The deviations from the equilibrium field

(i.e., disequilibrium) indicate processes of crystal accumulation or removal in the magmatic system as shown by arrows (Figure 7F). The vertical trend shown by the present olivine–liquid pairs is consistent with closed system differentiation processes (Figure 7F) and argues against magma mixing in the genesis of the studied rocks.

Mineralogical chemical compositions can reveal the history of magma cooling and crystallization conditions. Olivine, clinopyroxene, and plagioclase feldspars are important phases for understanding the temperature and pressure conditions of their crystallization from the parental mafic magmas. The temperature of olivine crystallization is estimated using Eq. 22 from Putirka (2008). The estimation indicates crystallization at 1,378–1,475 °C. The temperature of clinopyroxene crystallization is estimated using Eq. 33 from Putirka (2008), whereas the pressure of crystallization is estimated from the geobarometer of Neave and Putirka (2017). The geothermobarometer indicates crystallization at 1,137–1,214 °C under a pressure range of 3–9 kbar (Putirka, 2008; Neave and Putirka, 2017). The temperature and pressure of plagioclase crystallization are estimated using Eqs. 24a and 25a from Putirka (2008), respectively. The results indicate that plagioclase was crystallized at 1,096–1,108 °C under a pressure range of 5–7 kbar. Moreover, the plagioclase geo-hygrometer (model H of Putirka, 2005) indicates water contents of 0.63–1.41 wt%, suggesting crystallization under hydrous conditions. The temperature estimates suggest that the sequence of crystallization possibly began with olivine, then clinopyroxene, and soon after followed by plagioclase.

Nature of the mantle source

The trace and REE patterns (Figure 6) are identical for both eruptive lavas, suggesting generation from the same mantle source. Mantle sources can be distinguished using HFSE/LREE ratios (e.g., Nb/La) (Smith et al., 1999). The low Nb/La ratios (<1) indicate a lithospheric mantle source, whereas higher ratios (>1) reflect an asthenospheric mantle origin. So, the high Nb/La ratios (1.88–2.71) in the studied rocks are consistent with an OIB-like asthenospheric mantle source (Fitton et al., 1991; Smith et al., 1999). The Ba/Ce ratios (4.44–6.70) resemble those of OIB basalts (Halliday et al., 1995) and alkaline mafic lavas in the western Carpathian–Pannonian region (Ali et al., 2013). Their Lu/Hf and Nb/Ta ratios fall within the range of OIBs and show a tendency toward HIMU OIB-type basalts (Figure 8A; Pfänder et al., 2012). This tendency is also supported by Zr/Nb ratios (Figure 8B). These ratios are akin to those in continental basalts from Central Germany (Figures 8A, B). A negative K anomaly likely reflects the existence of a residual K-bearing phase (e.g., amphibole or phlogopite) in their mantle source (Wilson and Downes, 1991) or indicates that the mantle source itself is possibly depleted in K (Lustrino and Wilson, 2006).

Even though the asthenospheric mantle is basically garnet peridotite, anhydrous garnet peridotite is not a proper source for the alkaline basalts (e.g., Zeng et al., 2010) because high-pressure experimental studies on dry garnet peridotite do not yield melts of suitable basaltic composition (e.g., Hirose and Kushiro, 1993; Walter, 1998). The geo-hygrometer of the studied plagioclase reveals 0.63–1.41 wt% water content, suggesting crystallization from mafic magma having a hydrous mantle source (Putirka, 2005). Moreover, the super-chondritic Zr/Hf ratios (i.e., 41.2–48.1 vs. chondritic values = 38; Anders and Grevesse, 1989) of the studied rocks cannot be created by melting dry garnet peridotite since the peridotite has comparable partition coefficients for Zr and Hf (Salters et al., 2002). Thus, their super-chondritic Zr/Hf ratios might indicate carbonatitic fingerprints in their source region (Dupuy et al., 1992; Zeng et al., 2010). Moreover, the geochemical features of the studied lavas (e.g., high La/Yb_N, super-chondritic Zr/Hf ratios, and negative K anomalies) resemble those of carbonatites (Hoernle et al., 2002), suggesting that their mantle source was enriched by carbonatitic liquids (e.g., Chen et al., 2009 and Zeng et al., 2010) that are penetrated from great depths to generate carbonated silicate melts (Dasgupta et al., 2007). Pfänder et al. (2012) documented that the high Nb/Ta ratios in continental basalts compared to BSE are possibly confined to regions influenced by carbonatite metasomatism. This suggestion may indicate the high Nb/Ta ratios in the studied rocks when compared to BSE also reveal a carbonatitic signature in their mantle source. Moreover, the HIMU OIB-like signature (Figures 8A, B) possibly implies that these mafic lavas were produced from the partial melting of a peridotite mantle source that has been metasomatized by carbonatitic fluids (Weiss et al.,

2016). This is further supported by the SiO₂–CaO systematics, which indicates carbonated peridotite (<5% CO₂) partial melts (Dasgupta et al., 2007) (Figure 8C). They fall within the field of OIB-like lavas from the Canary and Galápagos Islands (Figure 8C), which show carbonatitic signatures in their mantle source regions (Dasgupta et al., 2007; Herzberg and Asimow, 2008). The total alkalis against the TiO₂ diagram (Figure 8D) show that the studied rocks plot in the zone of (K₂O + Na₂O)/TiO₂>1 and follow the variation trend of carbonated peridotite melts, which is different from that of hornblende and carbonated eclogite/pyroxenite melts. A carbonated peridotite mantle source was also suggested to explain the genesis of Cenozoic intraplate alkaline basalts from Shandong in North China (Zeng et al., 2010).

The probable CO₂ source is an undegassed reservoir having primordial carbon, unrelated to subducted-biogenic carbonate (Collerson et al., 2010 and refs. therein) since there are no signatures for the contribution of any subduction components in the source region. Gaillard et al. (2008) showed that anomalies that exist in the conductivity of the asthenospheric mantle are due to the occurrence of small amounts of carbonate melt (an average of 0.1 vol%) in the peridotite.

Melting conditions

Generally, the ratios of highly incompatible elements (e.g., Zr/Y) remain unchanged during crystal fractionation but vary with melting degrees in the basalt system (Nicholson and Latin, 1992). Zr is more incompatible in the mantle than Y; consequently, high Zr/Y ratios (8.6–11.5) in the studied rocks indicate that they were derived by low melting degrees. The La/Yb ratios are also sensitive to melting degree (Condie, 2003). So, the high La/Yb ratios (17.3–29.2) support lower degrees of melting as in average OIB (Condie, 2003). Moreover, the high concentrations of highly incompatible elements, such as Th and Zr, likely imply that they were generated by relatively low melting degrees of the peridotite mantle source (Tang et al., 2006). High Gd/Yb_N (2.6–4.0) and Tb/Yb_N (2.0–2.9) ratios suggest garnet-bearing peridotite source and argue for low degrees of partial melting (Walter, 1998; Wang et al., 2002). Moreover, the fractionated HREE patterns (Dy/Yb_N > 1) indicate that garnet was likely a residual phase in the source region during the partial melting process. Basalts with low HREE concentrations (e.g., Yb_N = 2.9–4.4) confirm residual garnet signature in their mantle source (Tang et al., 2006). The garnet signature indicates a deeper origin and melting at a depth greater than ~85 km at the garnet stability field.

The degree of melting represented by the alkaline basaltic rocks can be estimated based on the plot of La/Yb vs. Sm/Yb (Figure 9A; Zeng et al., 2010). The modeling reveals that those low degrees (4–10%) of batch melting of a garnet peridotite mantle source in the garnet stability field can produce the La/

Yb–Sm/Yb compositions of the studied rocks. The chondrite-normalized La/Yb_N and Dy/Yb_N ratios support the low melting degrees of 4–10%, where residual garnet is present at the source region (Figure 9B).

Tectonic implications and regional geodynamic setting

Clinopyroxene compositions of the studied rocks are typical for alkaline basaltic rocks formed in an anorogenic tectonic setting (Figures 4E, F; Leterrier et al., 1982). The Nb–Ta peak and K trough shown in the trace element patterns (Figure 6C) are also consistent with an anorogenic setting. The LREE-enriched patterns (La/Yb_N = 12.43–20.91) and absence of Eu anomalies in the REE patterns characterize the studied rocks and are compatible with OIB and intraplate alkaline basalts, suggesting a relation to the rift regime that occurred during the opening of the Red Sea (Sun and McDonough, 1989; Wittke and Mack, 1993). Moreover, the super-chondritic Zr/Hf ratios are comparable to OIB, intracontinental basalts, and Arabian intraplate volcanic rocks (Figure 6B), supporting the intraplate setting and rifting regime (Dupuy et al., 1992). Zr/Y ratios and Zr contents plot in the field of within-plate basalts (Figure 10A). The Th–Hf–Ta ternary plot indicates emplacement in the rift regime (Figure 10B). The rift-related signature in the intracontinental setting in the studied basanites is also confirmed by the La–Y–Nb relationship (Figure 5C). The trace and REE patterns are comparable to the Cenozoic rift-related intraplate basanites from Oman (Figures 6C, D). In summary, the studied basanites show OIB-like features and are akin to intracontinental basalts; they were formed during the rift regime associated with the opening of the Red Sea during the Tertiary.

The continental rifting system and related processes, such as rift origin and associated volcanism, structures, and crustal uplift, have been attributed to passive and/or active (i.e., plume) upwelling of the mantle source and are a matter of current debate (e.g., Courtillot et al., 1999; Buck, 2006; Farahat et al., 2006; Endress, 2010; Ali and Ntaflos, 2011; Chang and Van der Lee, 2011; Ali et al., 2013; Shallaly et al., 2013; Bosworth et al., 2015; Farahat et al., 2017; Ali and Alshammari, 2021). The Saudi Arabia basaltic flows, including the studied rocks, erupted during the Tertiary, coinciding with the prevalent volcanism in northern Africa and the Circum-Mediterranean regions (e.g., Lustrino and Wilson, 2007 and Endress et al., 2011). This volcanism is likely related to 1) continental rift which triggered localized lithospheric thinning and mantle decompression melting (e.g., Shaw et al., 2003; Ali and Ntaflos, 2011; Ali et al., 2013; Mohamed et al., 2014; Farahat et al., 2017) and/or 2) mantle plume source which resulted in an increase in mantle temperatures and provides metasomatic fluids to the overlying lithosphere mantle (e.g., Daradich et al., 2003; Chang and Van der Lee, 2011; Bosworth et al., 2015). Endress et al. (2011) suggested that

the geochemical characteristics of NE Egypt basaltic rocks likely reflect the contribution of both processes to their genesis.

The Red Sea rift development into an oceanic spreading ridge and related volcanism and crustal doming are frequently linked to the Afar plume (Volker et al., 1997; Courtillot et al., 1999; Ilani et al., 2001; Daradich et al., 2003; Farahat et al., 2006; Chang and Van der Lee, 2011). The southern Red Sea rift shows voluminous volcanism and significant crustal uplift, which characterizes both the African and Arabian plates (Baker et al., 1996; Hofmann et al., 1997). In contrast, the northern Red Sea rift shows variable volcanism and crustal uplift whereas the African plate is characterized by less voluminous and sporadic volcanism with less marked crustal doming than the Arabian plate.

The Red Sea magmatism, including that in Saudi Arabia, was sporadically distributed and less voluminous than that found on other rifted margins (Bosworth and Stockli, 2016). They are closely linked to the Red Sea rift during the Tertiary (e.g., Endress, 2010; Endress et al., 2011; Farahat et al., 2017). The pervasive Tertiary volcanism in northern Africa was related to shallow “plumelets” that impacted the base of the lithosphere, leading to temperature increase, and imported Afar plume-like components below NE Egypt or HIMU-like constituents in some regions (Endress et al., 2011). The basaltic volcanism in northern Egypt was also attributed to a “mini-plume” that accompanied the volcanic activity of the Red Sea margin (e.g., Saudi Arabia; Bosworth et al., 2015). However, Shallaly et al. (2013) and Farahat et al. (2017) provided evidence against a mantle plume beneath the Red Sea/Gulf of Suez rifts such as limited volcanic activity, minimal crustal uplift, and sporadic distribution of basaltic flows.

Several authors (Wilson and Guiraud, 1992; Wilson and Patterson, 2001; Beccaluva et al., 2008) supposed that at a low extension rate, volcanic activity provinces were likely linked to small plume upwelling from the asthenospheric mantle. The geochemical and isotopic characteristics of the largest intraplate volcanism on the Arabian plate (Harrat Ash Shaam, Jordan) suggest that the Afar plume was not channeled further northwards below the Arabian plate and could not play any role in the formation of northern Saudi Arabia and Jordan intraplate volcanism (Shaw et al., 2003). Accordingly, it seems that the studied basaltic volcanism was not affected by the Afar plume. Moreover, the studied basalts were generated by lower degrees of melting (4–10%; Figure 9), suggesting the low volume of the basaltic flows and low eruption rate (e.g., Shallaly et al., 2013; Farahat et al., 2017). This also indicates a low mantle potential temperature consistent with ambient mantle temperatures and passive mantle upwelling. Additional evidence such as the sporadic distribution of volcanism and the lack of regional uplift (Saleh et al., 2006) in Saudi Arabia argues against plume contribution. Moreover, seismic imaging of the mantle beneath the northern Red Sea and adjacent regions further support this implication and is unlikely to invoke mantle plume(s) introduced from the mantle transition zone (MTZ) or the lower mantle (Mohamed et al., 2014). Accordingly, the rift

structures most likely played an important role in the generation and emplacement of basaltic volcanism in the Arabian Shield of Saudi Arabia.

In conclusion, the basaltic volcanism in Saudi Arabia appears to be the product of melting asthenospheric mantle in response to the lithospheric extension that is spatially and temporally associated with the Red Sea rifting and triggered anorogenic mafic magmatism due to passive mantle upwelling beneath the Arabian Shield.

Concluding remarks

- 1-The studied basaltic rocks have similar REE patterns, suggesting derivation from a common mantle source.
- 2-Their OIB-like characteristics, silica undersaturation, and ratios of incompatible trace elements reflect an asthenospheric mantle source that was not affected by crustal and subduction components or by interaction with the lithospheric mantle.
- 3-High compatible trace element concentrations and low $\text{FeO}^{\text{total}}/\text{MgO}$ ratios reveal their relatively primitive nature and indicate minor crystal fractionation during the evolution of the studied rocks.
- 4- Geochemical features such as high $(\text{K}_2\text{O} + \text{Na}_2\text{O})/\text{TiO}_2$, Zr/Hf, and Nb/Ta ratios and negative K anomalies imply carbonated peridotite mantle source (<5% CO_2).
- 5- Highly incompatible elemental ratios and REE modeling suggest that they were derived by low partial melting degrees (4–10%) of a garnet-bearing lherzolite mantle source.
- 6- Basaltic volcanism in Saudi Arabia was likely produced by a melting asthenospheric mantle source due to lithospheric extension that is spatially and temporally associated with the Red Sea rift during the Cenozoic and triggered anorogenic mafic magmatism through passive mantle upwelling beneath the Arabian Shield.

Data availability statement

The original contributions presented in the study are included in the article/Supplementary Material; further inquiries can be directed to the corresponding author.

References

- Abu-Alam, T. S., Santosh, M., Brown, M., and Stüwe, K. (2013). Gondwana collision. *Mineralogy Petrology* 107, 631–634.
- Albarède, F. (1992). How deep do common basaltic magmas form and differentiate? *J. Geophys. Res.* 97, 10997–11009. doi:10.1029/91jb02927
- Ali, S., and Alshammari, A. S. (2021). Genesis of gabbroic intrusions in the Arabian Shield, Saudi Arabia: Mineralogical, geochemical and tectonic fingerprints of the neoproterozoic arc magmatism. *Geol. Mag.* 158, 1639–1656. doi:10.1017/S0016756821000182
- Ali, S., and Ntaflou, T. (2011). Alkali basalts from Burgenland, Austria: Petrological constraints on the origin of the westernmost magmatism in the Carpathian–Pannonian region. *Lithos* 121, 176–188. doi:10.1016/j.lithos.2010.11.001
- Ali, S., Ntaflou, T., and Upton, B. G. J. (2013). Petrogenesis and mantle source characteristics of Quaternary alkaline mafic lavas in the western Carpathian–Pannonian Region, Styria, Austria. *Chem. Geol.* 337–338, 99–113. doi:10.1016/j.chemgeo.2012.12.001

Author contributions

SA and SEA contributed to the conception and design of the study, organized the database, and performed the calculation and normalization of the analyses. SEA collected the rock samples and data. SA, SEA, and KA made the literature survey and helped with geological and field studies. SA wrote the first draft of the manuscript. SEA, MA, SAA, and KA wrote sections of the manuscript. All authors contributed to manuscript revision, read, and approved the submitted version.

Acknowledgments

We appreciate the essential comments and helpful reviews by three anonymous referees and by handling editor, Alcides Nobrega Sial, who significantly improved an early version of this manuscript.

Conflict of interest

The authors declare that the research was conducted in the absence of any commercial or financial relationships that could be construed as a potential conflict of interest.

Publisher's note

All claims expressed in this article are solely those of the authors and do not necessarily represent those of their affiliated organizations, or those of the publisher, the editors, and the reviewers. Any product that may be evaluated in this article, or claim that may be made by its manufacturer, is not guaranteed or endorsed by the publisher.

Supplementary material

The Supplementary Material for this article can be found online at: <https://www.frontiersin.org/articles/10.3389/feart.2022.921994/full#supplementary-material>

- Anders, E., and Grevesse, N. (1989). Abundances of the elements: Meteoritic and solar. *Geochimica Cosmochimica Acta* 53, 197–214. doi:10.1016/0016-7037(89)90286-x
- Bağcı, U., Alpaslan, M., Frei, R., Kurt, M., and Temel, A. (2011). Different degrees of partial melting of the enriched mantle source for Plio–Quaternary basic volcanism, toprakale (osmaniye) region, southern Turkey. *Turkish J. Earth Sci.* 20 (1), 5. doi:10.3906/yer-1003-30
- Baker, J., Snee, L., and Menzies, M. (1996). A brief Oligocene period of flood volcanism in Yemen: Implications for the duration and rate of continental flood volcanism at the afro–arabian triple junction. *Earth Planet. Sci. Lett.* 138, 39–55. doi:10.1016/0012-821x(95)00229-6
- Barth, M. G., McDonough, W. F., and Rudnick, R. L. (2000). Tracking the budget of Nb and Ta in the continental crust. *Chem. Geol.* 165, 197–213. doi:10.1016/S0009-2541(99)00173-4
- Beccaluva, L., Bianchini, G., Ellam, R. M., Marzola, M., Oun, K. M., Siena, F., et al. (2008). The role of HIMU metasomatic components in the north african lithospheric mantle: Petrological evidence from the gharyan lherzolite xenoliths, NW Libya. *Geol. Soc. Lond. Spec. Publ.* 293, 253–277. doi:10.1144/sp293.12
- Bosworth, W., and Stockli, D. F. (2016). Early magmatism in the greater Red Sea rift: Timing and significance. *Can. J. Earth Sci.* 53, 1158–1176. doi:10.1139/cjes-2016-0019
- Bosworth, W., Stockli, D. F., and Helgeson, D. E. (2015). Integrated outcrop, 3D seismic, and geochronologic interpretation of Red Sea dike–related deformation in the western desert, Egypt—The role of the 23 Ma cairo “mini-plume”. *J. Afr. Earth Sci.* 109, 107–119. doi:10.1016/j.jafrearsci.2015.05.005
- Büchl, A., Münker, C., Mezger, K., and Hofmann, A. W. (2002). High precision Nb/Ta and Zr/Hf ratios in global MORB. *Geochim. Cosmochim. Acta (Spec. Suppl.)* 66, A108.
- Buck, W. R. (2006). “The role of magma in the development of the Afro-Arabian rift system,” in *The Afar volcanic province within the East African rift system*. Editors G. Yirgu, C. J. Ebinger, and P. K. H. Maguire (London: Geological Society of London Special Publication), 43–54.
- Cabanis, B., and Lecolle, M. (1989). Le diagramme La/10-Y/15-Nb/8; un outil pour la discrimination des series volcaniques et la mise en evidence des processus de melange et/ou de contamination crustale. *Comptes Rendus l'Academie Sci. Ser. 2. Mec. Phys. Chim. Sci. l'Univers, Sci. Terre* 309 (20), 2023–2029.
- Chang, S., and Van der Lee, S. (2011). Mantle plumes and associated flow beneath Arabia and east Africa. *Earth Planet. Sci. Lett.* 302, 448–454. doi:10.1016/j.epsl.2010.12.050
- Chazot, G., and Bertrand, H. (1995). Genesis of silicic magmas during Tertiary continental rifting in Yemen. *Lithos* 36, 69–83. doi:10.1016/0024-4937(95)00012-5
- Chen, L.-H., Zeng, G., Jiang, S.-Y., Hofmann, A. W., Xu, X.-S., and Pan, M. B. (2009). Sources of anfangshan basalts: Subducted lower crust in the sulu UHP belt, China. *Earth Planet. Sci. Lett.* 286, 426–435. doi:10.1016/j.epsl.2009.07.006
- Collerson, K. D., Williams, Q., Ewart, A. E., and an Murphy, D. T. (2010). Origin of HIMU and EM-1 domains sampled by ocean island basalts, kimberlites and carbonatites: The role of CO₂-fluxed lower mantle melting in thermochemical upwellings. *Phys. Earth Planet. Interiors* 181, 112–131. doi:10.1016/j.pepi.2010.05.008
- Condie, K. C. (2003). Incompatible element ratios in oceanic basalts and komatiites: Tracking deep mantle sources and continental growth rates with time. *Geochem. Geophys. Geosyst.* 4 (1), 1–28. doi:10.1029/2002GC000333
- Condie, K. C. (1999). Mafic crustal xenoliths and the origin of the lower continental crust. *Lithos* 46 (1), 95–101. doi:10.1016/S0024-4937(98)00056-5
- Courtillot, V., Jaupart, C., Manighetti, I., Tapponnier, P., and Besse, J. (1999). On causal links between flood basalts and continental breakup. *Earth Planet. Sci. Lett.* 166, 177–195. doi:10.1016/S0012-821x(98)00282-9
- Daradich, A., Mitrovica, J. X., Pysklywec, R. N., Willett, S. D., and Forte, A. M. (2003). Mantle flow, dynamic topography, and rift–flank uplift of Arabia. *Geol.* 31, 901–904. doi:10.1130/g19661.1
- Dasgupta, R., Hirschmann, M. M., and Smith, N. D. (2007). Partial melting experiments of peridotite+CO₂ at 3 GPa and genesis of alkalic ocean island basalts. *J. Petrology* 48, 2093–2124. doi:10.1093/petrology/egm053
- Dasgupta, R., Hirschmann, M. M., and Stalker, K. (2006). Immiscible transition from carbonate–rich to silicate–rich melts in the 3 GPa melting interval of eclogite+CO₂ and genesis of silica–undersaturated ocean island lavas. *J. Petrology* 47, 647–671. doi:10.1093/petrology/egi088
- Deer, W. A., Howie, R. A., and Zussman, J. (1992). *An introduction to the rock-forming minerals*. London: Longman Scientific and Technical Publishing.
- Dupuy, C., Liotard, J. M., and Dosta, J. (1992). Zr/Hf fractionation in intraplate basaltic rocks: Carbonate metasomatism in the mantle source. *Geochim. Cosmochim. Acta* 56, 2417–2423. doi:10.1016/0016-7037(92)90198-r
- Ekren, E. B., Vaslet, D., Berthiaux, A., Le Strat, P., and Fourniguet, J. (1987). *Geologic map of the ha'il quadrangle, sheet 27E, kingdom of Saudi Arabia, scale 1: 250,000*. Jeddah: Deputy Ministry for Mineral Resources, Kingdom of Saudi Arabia Ministry of Petroleum and Mineral Resources.
- Endress, C., Furman, T., Abu El-Rus, M. A., and Hanan, B. B. (2011). “Geochemistry of 24 Ma basalts from NE Egypt: Source components and fractionation history,”. Editors D. J. J. Van Hinsbergen, S. J. H. Buitert, T. H. Torsvik, C. Gaina, and S. J. Webb (London, United Kingdom: The Geological Society Burlington House Piccadilly), *Form. Evol. Afr. A Synop.* 3.8 *Ga Earth Hist.* 357, 265–283.
- Endress, C. (2010). *Geochemistry of 24 Ma basalts from northeast Egypt: Implications for widespread magmatism in northern Africa*. M.Sc. Thesis. Pennsylvania State University, 162.
- Farahat, E. S., Ali, S., and Hauzenberger, C. (2017). Red Sea rift-related quseir basalts, central eastern desert, Egypt: Petrogenesis and tectonic processes. *Bull. Volcanol.* 79, 9. doi:10.1007/s00445-016-1092-6
- Farahat, E. S., and Ali, S. (2019). Origin and geotectonic evolution of Mir Tertiary basaltic andesite dykes, Western Desert, Egypt: Constraints from mineral and bulk-rock chemistry. *Geol. J.* 54, 2274–2287. doi:10.1002/gj.3296
- Farahat, E. S., Ghani, M. S. A., Aboazom, A. S., and Asran, A. M. H. (2006). Mineral chemistry of Al haruj low–volcanicity rift basalts, Libya: Implications for petrogenetic and geotectonic evolution. *J. Afr. Earth Sci.* 45 (2), 198–212. doi:10.1016/j.jafrearsci.2006.02.007
- Fitton, J. G., James, D., and Leeman, W. P. (1991). Basic magmatism associated with late cenozoic extension in the western United States: Compositional variations in space and time. *J. Geophys. Res.* 96, 13693–13711. doi:10.1029/91jb00372
- Gaillard, F., Malki, M., Lacono–Marziano, G., Pichavant, M., and Scaillet, B. (2008). Carbonatite melts and electrical conductivity in the asthenosphere. *Science* 322, 1363–1365. doi:10.1126/science.1164446
- Girdler, R. W., and Styles, P. (1974). Two stage Red Sea floor spreading. *Nature* 247, 7–11. doi:10.1038/247007a0
- Greenwood, W. R. (1974). The Hail arch- a key to deformation of the arabian Shield during evolution of the Red Sea rift: Saudi arabian directorate Ge. *Mineral. Resour. Bull.* 7, 5.
- Halliday, A. N., Lee, D.-C., Tommasini, S., Davies, G. R., Paslick, C. R., Fitton, J. D., et al. (1995). Incompatible trace elements in OIB and MORB and source enrichment in the sub-oceanic mantle. *Earth Planet. Sci. Lett.* 133, 379–395. doi:10.1016/0012-821x(95)00097-v
- Herzberg, C., and Asimov, P. D. (2008). Petrology of some oceanic island basalts: PRIMELT2.XLS software for primary magma calculation. *Geochem. Geophys. Geosyst.* 9, 332. doi:10.1029/2008GC002057
- Hirose, K., and Kushiro, I. (1993). Partial melting of dry peridotites at high pressures: Determination of compositions of melts segregated from peridotite using aggregates of diamond. *Earth Planet. Sci. Lett.* 114, 477–489. doi:10.1016/0012-821x(93)90077-m
- Hoernle, K., Tilton, G., Le Bas, M. J., Duggen, S., and Garbe-Schonberg, D. (2002). Geochemistry of oceanic carbonatites compared with continental carbonatites: Mantle recycling of oceanic crustal carbonate. *Contrib. Mineral. Pet.* 142, 520–542. doi:10.1007/s004100100308
- Hofmann, A. W., Jochum, K. P., Seufert, M., and White, W. M. (1986). Nb and Pb in oceanic basalts, new constraints on mantle evolution. *Earth Planet. Sci. Lett.* 79, 33–45. doi:10.1016/0012-821x(86)90038-5
- Hofmann, C., Courtillot, V., Férand, G., Rochette, P., Yirgu, G., Ketefo, E., et al. (1997). Timing of the Ethiopian flood basalt event and implications for plume birth and global change. *Nature* 389, 838–841. doi:10.1038/39853
- Ilani, S., Harlavan, Y., Tarawneh, K., Rabba, I., Weinberger, R., Ibrahim, K., et al. (2001). New K–Ar ages of basalts from the harrat Ash Shaam volcanic field in Jordan: Implications for the span and duration of the upper-mantle upwelling beneath the western Arabian Plate. *Geol.* 29, 171–174. doi:10.1130/0091-7613(2001)029<0171:nkaaob>2.0.co;2
- Johnson, P. R., and Woldehaimanot, B. (2003). “Development of the arabian–nubian Shield: Perspectives on accretion and deformation in the northern east african orogen and assembly of Gondwana,” in *Proterozoic east Gondwana: Supercontinent assembly and breakup*. Editors M. Yoshida and B. F. Windley and S. Dasgupta (London, United Kingdom: The Geological Society Burlington House Piccadilly), 289–326.
- Kamenetsky, V. S., Elburg, M., Arculus, R., and Thomas, R. (2006). Magmatic origin of low-Ca olivine in subduction-related magmas: Co-Existence of contrasting magmas. *Chem. Geol.* 233, 346–357. doi:10.1016/j.chemgeo.2006.03.010
- Krienitz, M. S., Haase, K. M., Mezger, K., Eckardt, V., and Shaikh-Mashail, M. A. (2006). Magma genesis and crustal contamination of continental intraplate lavas in

- northwestern Syria. *Contrib. Mineral. Pet.* 151, 698–716. doi:10.1007/s00410-006-0088-1
- Krienitz, M. S., Haase, K. M., Mezger, K., and Shaikh-Mashail, M. A. (2007). Magma genesis and mantle dynamics at the Harrat Ash Shamah volcanic field (Southern Syria). *J. Petrology* 48, 1513–1542. doi:10.1093/petrology/egm028
- Krienitz, M. S., Haase, K. M., Mezger, K., van den Bogaard, P., Thiemann, V., and Shaikh-Mashail, M. A. (2009). Tectonic events, continental intraplate volcanism and mantle plume activity in northern Arabia: Constraints from geochemistry and Ar–Ar dating of Syrian lavas. *Geochem. Geophys. Geosyst.* 10 (4). doi:10.1029/2008gc002254
- Le Maitre, R., Bateman, P., Dudek, A., Keller, J., Lameyre, J., Le Bas, M., et al. (1989). in *A classification of igneous rocks and glossary of terms: Recommendations of the International Union of Geological Sciences Subcommission on the Systematics of igneous rocks*. Editor R. W. Le Maitre (Oxford: Blackwell), 193.
- Leterrier, J., Maury, R. C., Thonon, P., Girard, D., and Marchal, M. (1982). Clinopyroxene composition as a method of identification of the magmatic affinities of paleo-volcanic series. *Earth Planet. Sci. Lett.* 59, 139–154. doi:10.1016/0012-821x(82)90122-4
- Lustrino, M., and Wilson, M. (2007). The circum-Mediterranean anorogenic Cenozoic igneous province. *Earth-Science Rev.* 81, 1–65. doi:10.1016/j.earscirev.2006.09.002
- McKenzie, D. P., and Bickle, M. J. (1988). The volume and composition of melt generated by extension of the lithosphere. *J. Petrology* 29 (3), 625–679. doi:10.1093/petrology/29.3.625
- McKenzie, D. P., Davies, D., and Molnar, P. (1970). Plate tectonics of the Red Sea and east Africa. *Nature* 226, 243–248. doi:10.1038/226243a0
- Meert, J. G. (2003). A synopsis of events related to the assembly of eastern Gondwana. *Tectonophysics* 362, 1–40. doi:10.1016/s0040-1951(02)00629-7
- Mohamed, A. A., Gao, S. S., Elsheikh, A. A., Liu, K. H., Yu, Y., and Fat-Helbary, R. E. (2014). Seismic imaging of mantle transition zone discontinuities beneath the northern Red Sea and adjacent areas. *Geophys. J. Int.* 199, 648–657. doi:10.1093/gji/ggu284
- Morimoto, N., Fabries, J., Ferguson, A. K., Ginzburg, I. V., Ross, M., Seifert, F. A., et al. (1988). Nomenclature of pyroxenes. *bulmi.* 52, 535–550. doi:10.3406/bulmi.1988.8099
- Münker, C., Pfänder, J. A., Weyer, S., Büchl, A., Kleine, T., and Mezger, K. (2003). Evolution of planetary cores and the Earth–Moon system from Nb/Ta systematics. *Science* 301, 84–87. doi:10.1126/science.1084662
- Nasir, S., and Stern, R. J. (2012). Lithospheric petrology of the eastern Arabian plate: Constraints from Al-ashkhara (Oman) xenoliths. *Lithos* 132–133, 98–112. doi:10.1016/j.lithos.2011.11.011
- Nicholson, H., and Latin, D. (1992). Olivine tholeiites from Krafla, Iceland: Evidence for variations in melt fraction within a plume. *J. Petrology* 33, 1105–1124. doi:10.1093/petrology/33.5.1105
- Pallister, J. S., McCausland, W. A., Jónsson, S., Lu, Z., Zahran, H. M., Hadidy, S. E., et al. (2010). Broad accommodation of rift-related extension recorded by dyke intrusion in Saudi Arabia. *Nat. Geosci.* 3, 705–712. doi:10.1038/ngeo966
- Pearce, J. A. (2008). Geochemical fingerprinting of oceanic basalts with applications to ophiolite classification and the search for Archean oceanic crust. *Lithos* 100, 14–48. doi:10.1016/j.lithos.2007.06.016
- Pearce, J. A., and Norry, M. L. (1979). Petrogenetic implications of Ti, Zr, Y, and Nb variations in volcanic rocks. *Contr. Mineral. Pet.* 69, 33–47. doi:10.1007/bf00375192
- Pfänder, J. A., Münker, C., Stracke, A., and Mezger, K. (2007). Nb/Ta and Zr/Hf in ocean island basalts—implications for crust–mantle differentiation and the fate of Niobium. *Earth Planet. Sci. Lett.* 254, 158–172. doi:10.1016/j.epsl.2006.11.027
- Pfänder, J., Jung, S., Münker, C., Stracke, A., and Mezger, K. (2012). A possible high Nb/Ta reservoir in the continental lithospheric mantle and consequences on the global Nb budget—Evidence from continental basalts from Central Germany. *Geochimica Cosmochimica Acta* 77, 232–251. doi:10.1016/j.gca.2011.11.017
- Pik, R., Deniel, C., Coulon, C., Yirgu, G., and Marty, B. (1999). Isotopic and trace element signatures of Ethiopian flood basalts: Evidence for plume lithosphere interactions. *Geochim. Cosmochim. Acta* 63, 2263–2279. doi:10.1016/s0016-7037(99)00141-6
- Pilet, S., Baker, M. B., and Stolper, E. M. (2008). Metasomatized lithosphere and the origin of alkaline Lavas. *Science* 320, 916–919. doi:10.1126/science.1156563
- Polat, A., and Hofmann, A. W. (2003). Alteration and geochemical patterns in the 3.7–3.8 Ga Isua greenstone belt, West Greenland. *Precambrian Res.* 126, 197–218. doi:10.1016/s0301-9268(03)00095-0
- Roeder, P. L., and Emslie, R. F. (1970). Olivine-liquid equilibrium. *Contr. Mineral. Pet.* 29, 275–289. doi:10.1007/bf00371276
- Rudnick, R. L., and Fountain, D. M. (1995). Nature and composition of the continental crust: A lower crustal perspective. *Rev. Geophys.* 33, 267–309. doi:10.1029/95rg01302
- Rudnick, R. L., Gao, S., and Rudnick, R. L. (2003). “Composition of the continental crust,” in *The crust. Treatise on Geochemistry*. Editors H. D. Holland and K. K. Turekian (Oxford: Elsevier–Pergamon), 3, 1–64., (Ed),
- Saleh, S., Jahr, T., Jentzsch, G., Saleh, A., and Abou Ashour, N. M. (2006). Crustal evaluation of the northern Red Sea rift and gulf of Suez, Egypt from geophysical data: 3-dimensional modeling. *J. Afr. Earth Sci.* 45, 257–278. doi:10.1016/j.jafrearsci.2006.02.001
- Salteras, V. J. M., Longhi, J. E., and Bizimis, M. (2002). Near mantle solidus trace element partitioning at pressures up to 3.4 GPa. *Geochem. Geophys. Geosyst.* 3 (7), 1–23. doi:10.1029/2001GC000148
- Shallal, N. A., Beier, C., Haase, K. M., and Hamed, M. S. (2013). Petrology and geochemistry of the tertiary Suez rift volcanism, Sinai, Egypt. *J. Volcanol. Geotherm. Res.* 267, 119–137. doi:10.1016/j.jvolgeores.2013.10.005
- Shaw, J. E., Baker, J. A., Menzies, M. A., Thirlwall, M. F., and Ibrahim, K. M. (2003). Petrogenesis of the largest intraplate volcanic field on the Arabian plate (Jordan): A mixed lithosphere–asthenosphere source activated by lithospheric extension. *J. Petrology* 44, 1657–1679. doi:10.1093/petrology/egg052
- Smith, E. I., Sánchez, A., Walker, J. D., and Wang, K. (1999). Geochemistry of mafic magmas in the hurricane volcanic field, Utah: Implications for small- and large-scale chemical variability of the lithospheric mantle. *J. Geol.* 107, 433–448. doi:10.1086/314355
- Stein, M., and Hofmann, A. W. (1992). Fossil plume head beneath the Arabian lithosphere? *Earth planet. Sci. Lett.* 114, 193–209. doi:10.1016/0012-821x(92)90161-n
- Stern, R. J. (2002). Crustal evolution in the east african orogen: A neodymium isotopic perspective. *J. Afr. Earth Sci.* 34, 109–117. doi:10.1016/s0899-5362(02)00012-x
- Stern, R. J., and Johnson, P. R. (2019). “Constraining the opening of the Red Sea: Evidence from the neoproterozoic margins and cenozoic magmatism for a volcanic rifted margin,” in *Geological setting, palaeoenvironment and archaeology of the Red Sea*. Editors N. Rasul and I. Stewart (Cham: Springer). doi:10.1007/978-3-319-99408-6_4
- Stern, R. J., and Johnson, P. R. (2010). Continental lithosphere of the Arabian Plate: A geologic, petrologic, and geophysical synthesis. *Earth. Sci. Rev.* 101, 29–67. doi:10.1016/j.earscirev.2010.01.002
- Stoeser, D. B., and Elliott, J. E. (1985). Reconnaissance geology of the Al Qasr quadrangle, sheet 27/41C, kingdom of Saudi Arabia. *U. S. Geol. Surv. Open-File Rep.* 85-668, 51. Deputy Ministry for Mineral Resources, Saudi Arabia.
- Stoeser, D. B., and Frost, C. D. (2006). Nd, Pb, Sr, and O isotopic characterization of Saudi Arabian Shield terranes. *Chem. Geol.* 226, 163–188. doi:10.1016/j.chemgeo.2005.09.019
- Sun, S. S., and McDonough, W. F. (1989). “Chemical and isotopic systematics of oceanic basalts: Implications for mantle composition and processes,”. Editors A. D. Saunders and M. J. Norry (London: Geological Society London, Special Publication), 42, 313–345. *Magmatism Ocean Basins*
- Tang, Y.-J., Zhang, H.-F., and Ying, J.-F. (2006). Asthenosphere–lithospheric mantle interaction in an extensional regime: Implication from the geochemistry of cenozoic basalts from taihang mountains, north China craton. *Chem. Geol.* 233, 309–327. doi:10.1016/j.chemgeo.2006.03.013
- Taylor, S. R., and McLennan, S. M. (1995). *The continental crust: Its composition and evolution*. Oxford: Blackwell, 1–312.
- Thompson, R. N., and Gibson, S. A. (2000). Transient high temperatures in mantle plume heads inferred from magnesium olivines in Phanerozoic picrites. *Nature* 407, 502–506. doi:10.1038/35035058
- Vinet, N., Molina, P., Flemming, R. L., Houde, V., Morgado, E., Barra, F., et al. (2015). Quantification and origin of the intracrystalline deformation of olivine from basalts of the andean southern volcanic zone: A multidisciplinary study. XIV congreso geológico chileno. *La Serena Oct.* 2015.
- Volker, F., Altherr, R., Jochum, K. P., and McCulloch, M. T. (1997). Quaternary volcanic activity of the southern Red Sea: New data and assessment of models on magma sources and Afar plume–lithosphere interaction. *Tectonophysics* 278, 15–29. doi:10.1016/S0040-1951(97)00092-9
- Walter, M. J. (1998). Melting of garnet peridotite and the origin of komatiite and depleted lithosphere. *J. Petrology* 39, 29–60. doi:10.1093/petroj/39.1.29
- Wang, K., Plank, T., Walker, J. D., and Smith, E. I. (2002). A mantle melting profile across the Basin and Range, SW USA. *J. Geophys. Res.* 973 (B1), 107. doi:10.1029/2001JB0002092017
- Weiss, Y., Class, C., Goldstein, S. L., and Hanyu, T. (2016). Key new pieces of the HIMU puzzle from olivines and diamond inclusions. *Nature* 537, 666–670. doi:10.1038/nature19113

Wilson, M., and Downes, H. (1991). Tertiary–quaternary extension-related alkaline magmatism in western and central Europe. *J. Petrology* 32, 811–849. doi:10.1093/ptrology/32.4.811

Wilson, M., and Guiraud, R. (1992). Magmatism and rifting in western and central Africa, from late Jurassic to recent times. *Tectonophysics* 213, 203–225. doi:10.1016/0040-1951(92)90259-9

Wilson, M., and Patterson, R. (2001). “Intraplate magmatism related to short wavelength convective instabilities in the upper mantle: Evidence from the tertiary–quaternary volcanic province of western and central Europe.”, Editors R. E. Ernst and K. L. Buchan (Washington D. C: Geological Society of America Special Paper), 352, 37–58. *Mantle Plumes Their Identif. through Time*

Witte, M., Jung, S., Pfänder, J. A., Romer, R. L., Mayer, B., and Garbe-Schönberg, D. (2017). OIB signatures in basin-related lithosphere-derived alkaline basalts from

the Batain basin (Oman) — constraints from $^{40}\text{Ar}/^{39}\text{Ar}$ ages and Nd–Sr–Pb–Hf isotopes. *Lithos* 286–287, 109–124. doi:10.1016/j.lithos.2017.05.024

Wittke, J. H., and Mack, L. E. (1993). OIB-like mantle source for continental alkaline rocks of the balcones province, Texas: Trace-element and isotopic evidence. *J. Geol.* 101, 333–344. doi:10.1086/648227

Wood, D. A. (1980). The application of a Th–Hf–Ta diagram to problems of tectonomagmatic classification and to establishing the nature of crustal contamination of basaltic lavas of the British Tertiary volcanic province. *Earth Planet. Sci. Lett.* 50 (1), 11–30. doi:10.1016/0012-821x(80)90116-8

Zeng, G., Chen, L.-H., Xu, X.-S., Jiang, S.-Y., and Hofmann, A. W. (2010). Carbonated mantle sources for Cenozoic intraplate alkaline basalts in Shandong, North China. *Chem. Geol.* 273, 35–45. doi:10.1016/j.chemgeo.2010.02.009